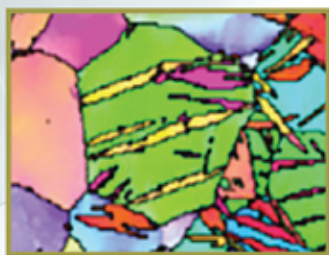
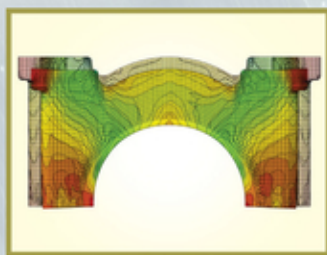
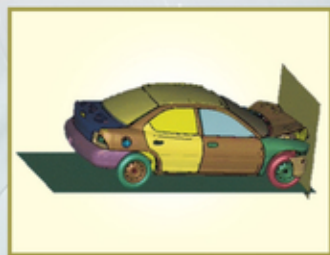


Edited by
Mark F. Horstemeyer

INTEGRATED COMPUTATIONAL MATERIALS ENGINEERING (ICME) FOR METALS

Concepts and Case Studies



WILEY

**Integrated Computational Materials
Engineering (ICME) for Metals**

Integrated Computational Materials Engineering (ICME) for Metals

Concepts and Case Studies

Edited by
Mark F. Horstemeyer

WILEY

This edition first published 2018
© 2018 John Wiley & Sons, Inc

All rights reserved. No part of this publication may be reproduced, stored in a retrieval system, or transmitted, in any form or by any means, electronic, mechanical, photocopying, recording or otherwise, except as permitted by law. Advice on how to obtain permission to reuse material from this title is available at <http://www.wiley.com/go/permissions>.

The right of Mark F. Horstemeyer to be identified as the editor of this work has been asserted in accordance with law.

Registered Office

John Wiley & Sons, Inc., 111 River Street, Hoboken, NJ 07030, USA

Editorial Office

111 River Street, Hoboken, NJ 07030, USA

For details of our global editorial offices, customer services, and more information about Wiley products visit us at www.wiley.com.

Wiley also publishes its books in a variety of electronic formats and by print-on-demand. Some content that appears in standard print versions of this book may not be available in other formats.

Limit of Liability/Disclaimer of Warranty

The publisher and the authors make no representations or warranties with respect to the accuracy or completeness of the contents of this work and specifically disclaim all warranties, including without limitation any implied warranties of fitness for a particular purpose. This work is sold with the understanding that the publisher is not engaged in rendering professional services. The advice and strategies contained herein may not be suitable for every situation. In view of ongoing research, equipment modifications, changes in governmental regulations, and the constant flow of information relating to the use of experimental reagents, equipment, and devices, the reader is urged to review and evaluate the information provided in the package insert or instructions for each chemical, piece of equipment, reagent, or device for, among other things, any changes in the instructions or indication of usage and for added warnings and precautions. The fact that an organization or website is referred to in this work as a citation and/or potential source of further information does not mean that the author or the publisher endorses the information the organization or website may provide or recommendations it may make. Further, readers should be aware that websites listed in this work may have changed or disappeared between when this work was written and when it is read. No warranty may be created or extended by any promotional statements for this work. Neither the publisher nor the author shall be liable for any damages arising herefrom.

Library of Congress Cataloging-in-Publication Data:

Names: Horstemeyer, Mark F. (Mark Fredrick), 1962- editor.

Title: Integrated computational materials engineering (ICME) for metals :
case studies / edited by Mark F. Horstemeyer.

Description: Hoboken, NJ : John Wiley & Sons, 2018. | Includes
bibliographical references and index. |

Identifiers: LCCN 2017043470 (print) | LCCN 2017056730 (ebook) | ISBN
9781119018391 (pdf) | ISBN 9781119018384 (epub) | ISBN 9781119018360
(cloth)

Subjects: LCSH: Metals—Mathematical models. | Materials science—Data
processing. | Metal products—Computer simulation. | Multiscale modeling.

Classification: LCC TA459 (ebook) | LCC TA459 .I4515 2018 (print) | DDC
620.1/6—dc23

LC record available at <https://lccn.loc.gov/2017043470>

Cover Design: Wiley

Cover Image: Courtesy of Mark F. Horstemeyer; Background: © pawel.gau/Getty Images

Set in 10/12pt WarnockPro by SPi Global, Chennai, India

Printed in the United States of America

10 9 8 7 6 5 4 3 2 1

Contents

List of Contributors *xix*

Foreword *xxvii*

Preface *xxix*

1	Definition of ICME	1
	<i>Mark F. Horstemeyer and Satyam Sahay</i>	
1.1	What ICME Is NOT	1
1.1.1	Adding Defects into a Mechanical Theory	1
1.1.2	Adding Microstructures to Finite Element Analysis (FEA)	2
1.1.3	Comparing Modeling Results to Structure–Property Experimental Results	2
1.1.4	Computational Materials	2
1.1.5	Design Materials for Manufacturing (Process–Structure–Property Relationships)	3
1.1.6	Simulation through the Process Chain	3
1.2	What ICME Is	4
1.2.1	Background	4
1.2.2	ICME Definition	5
1.2.3	Uncertainty	8
1.2.4	ICME Cyberinfrastructure	9
1.3	Industrial Perspective	10
1.4	Summary	15
	References	15

Section I Body-Centered Cubic Materials **19**

2	From Electrons to Atoms: Designing an Interatomic Potential for Fe–C Alloys	21
	<i>Laalitha S. I. Liyanage, Seong-Gon Kim, Jeff Houze, Sungho Kim, Mark A. Tschopp, Michael I. Baskes, and Mark F. Horstemeyer</i>	
2.1	Introduction	21
2.2	Methods	23

2.2.1	MEAM Calculations	24
2.2.2	DFT Calculations	24
2.3	Single-Element Potentials	25
2.3.1	Energy versus Volume Curves	25
2.3.1.1	Single-Element Material Properties	29
2.4	Construction of Fe–C Alloy Potential	29
2.5	Structural and Elastic Properties of Cementite	35
2.5.1	Single-Crystal Elastic Properties	36
2.5.2	Polycrystalline Elastic Properties	37
2.5.3	Surface Energies	37
2.5.4	Interstitial Energies	38
2.6	Properties of Hypothetical Crystal Structures	38
2.6.1	Energy versus Volume Curves for B_1 and L_{12} Structures	38
2.6.2	Elastic Constants for B_1 and L_{12} Structures	40
2.7	Thermal Properties of Cementite	40
2.7.1	Thermal Stability of Cementite	40
2.7.2	Melting Temperature Simulation	40
2.7.2.1	Preparation of Two-Phase Simulation Box	41
2.7.2.2	Two-Phase Simulation	41
2.8	Summary and Conclusions	44
	Acknowledgments	45
	References	45
3	Phase-Field Crystal Modeling: Integrating Density Functional Theory, Molecular Dynamics, and Phase-Field Modeling	49
	<i>Mohsen Asle Zaeem and Ebrahim Asadi</i>	
3.1	Introduction to Phase-Field and Phase-Field Crystal Modeling	49
3.2	Governing Equations of Phase-Field Crystal (PFC) Models Derived from Density Functional Theory (DFT)	53
3.2.1	One-Mode PFC model	53
3.2.2	Two-Mode PFC Model	55
3.3	PFC Model Parameters by Molecular Dynamics Simulations	57
3.4	Case Study: Solid–Liquid Interface Properties of Fe	59
3.5	Case Study: Grain Boundary Free Energy of Fe at Its Melting Point	63
3.6	Summary and Future Directions	65
	References	66
4	Simulating Dislocation Plasticity in BCC Metals by Integrating Fundamental Concepts with Macroscale Models	71
	<i>Hojun Lim, Corbett C. Battaile, and Christopher R. Weinberger</i>	
4.1	Introduction	71
4.2	Existing BCC Models	73
4.3	Crystal Plasticity Finite Element Model	85
4.4	Continuum-Scale Model	90

4.5	Engineering Scale Applications	92
4.6	Summary	99
	References	101
5	Heat Treatment and Fatigue of a Carburized and Quench Hardened Steel Part	107
	<i>Zhichao (Charlie) Li and B. Lynn Ferguson</i>	
5.1	Introduction	107
5.2	Modeling Phase Transformations and Mechanics of Steel Heat Treatment	108
5.3	Data Required for Modeling Quench Hardening Process	112
5.3.1	Dilatometry Data	113
5.3.2	Mechanical Property Data	114
5.3.3	Thermal Property Data	114
5.3.4	Process Data	114
5.3.5	Furnace Heating	115
5.3.6	Gas Carburization	116
5.3.7	Immersion Quenching	116
5.4	Heat Treatment Simulation of a Gear	118
5.4.1	Description of Gear Geometry, FEA Model, and Problem Statement	119
5.4.2	Carburization and Air Cooling Modeling	120
5.4.3	Quench Hardening Process Modeling	122
5.4.4	Comparison of Model and Experimental Results	128
5.4.5	Tooth Bending Fatigue Data and Loading Model	129
5.5	Summary	132
	References	134
6	Steel Powder Metal Modeling	137
	<i>Youssef Hammi, Tonya Stone, Haley Doude, L. Arias Tucker, P. G. Allison, and Mark F. Horstemeyer</i>	
6.1	Introduction	137
6.2	Material: Steel Alloy	137
6.3	ICME Modeling Methodology	139
6.3.1	Compaction	139
6.3.1.1	Macroscale Compaction Model	139
6.3.1.2	Compaction Model Calibration	146
6.3.1.3	Validation	146
6.3.1.4	Compaction Model Sensitivity and Uncertainty Analysis	148
6.3.2	Sintering	151
6.3.2.1	Atomistic	152
6.3.2.2	Theory and Simulations	152
6.3.2.3	Sintering Structure–Property Relations	155
6.3.2.4	Sintering Constitutive Modeling	160
6.3.2.5	Sintering Model Implementation and Calibration	163

- 6.3.2.6 Sintering Validation for an Automotive Main Bearing Cap 165
- 6.3.3 Performance/Durability 165
 - 6.3.3.1 Monotonic Conditions 167
 - 6.3.3.2 Plasticity-Damage Structure–Property Relations 167
 - 6.3.3.3 Plasticity-Damage Model and Calibration 168
 - 6.3.3.4 Validation and Uncertainty 173
 - 6.3.3.5 Main Bearing Cap 174
 - 6.3.3.6 Fatigue 176
- 6.3.4 Optimization 188
 - 6.3.4.1 Design of Experiments (DOE) 189
 - 6.3.4.2 Results and Discussion 191
- 6.4 Summary 193
 - References 194

7 Microstructure-Sensitive, History-Dependent Internal State Variable Plasticity-Damage Model for a Sequential Tubing Process 199

Heechen E. Cho, Youssef Hammi, David K. Francis, Tonya Stone, Yuxiong Mao, Ken Sullivan, John Wilbanks, Robert Zelinka, and Mark F. Horstemeyer

- 7.1 Introduction 199
- 7.2 Internal State Variable (ISV) Plasticity-Damage Model 202
 - 7.2.1 History Effects 202
 - 7.2.2 Constitutive Equations 202
- 7.3 Simulation Setups 207
- 7.4 Results 209
 - 7.4.1 ISV Plasticity-Damage Model Calibration and Validation 209
 - 7.4.2 Simulations of the Forming Process (Step 1) 210
 - 7.4.3 Simulations of Sizing Process (Step 3) 213
 - 7.4.4 Simulations of First Annealing Process (Step 4) 217
 - 7.4.5 Simulations of Drawing Processes (Steps 5 and 6) 225
 - 7.4.6 Simulations of Second Annealing Process (Step 7) 230
- 7.5 Conclusions 232
 - References 233

Section II Hexagonal Close Packed (HCP) Materials 235

8 Electrons to Phases of Magnesium 237

Bi-Cheng Zhou, William Yi Wang, Zi-Kui Liu, and Raymundo Arroyave

- 8.1 Introduction 237
- 8.2 Criteria for the Design of Advanced Mg Alloys 238
- 8.3 Fundamentals of the ICME Approach Designing the Advanced Mg Alloys 238
 - 8.3.1 Roadmap of ICME Approach 238
 - 8.3.2 Fundamentals of Computational Thermodynamics 239
 - 8.3.3 Electronic Structure Calculations of Materials Properties 241

8.3.3.1	First-Principles Calculations for Finite Temperatures	242
8.3.3.2	First-Principles Calculations of Solid Solution Phase	244
8.3.3.3	First-Principles Calculations of Interfacial Energy	245
8.3.3.4	Equation of States (EOSs) and Elastic Moduli	245
8.3.3.5	Deformation Electron Density	246
8.3.3.6	Diffusion Coefficient	246
8.4	Data-Driven Mg Alloy Design – Application of ICME Approach	248
8.4.1	Electronic Structure	248
8.4.2	Thermodynamic Properties	253
8.4.3	Phase Stability and Phase Diagrams	253
8.4.3.1	Database Development	253
8.4.3.2	Application of CALPHAD in Mg Alloy Design	255
8.4.4	Kinetic Properties	260
8.4.5	Mechanical Properties	262
8.4.5.1	Elastic Constants	262
8.4.5.2	Stacking Fault Energy and Ideal Strength Impacted by Alloying Elements	265
8.4.5.3	Prismatic and Pyramidal Slips Activated by Lattice Distortion	270
8.5	Outlook/Future Trends	272
	Acknowledgments	272
	References	273
9	Multiscale Statistical Study of Twinning in HCP Metals	283
	<i>Carlos N. Tomé, Irene J. Beyerlein, Rodney J. McCabe, and Jian Wang</i>	
9.1	Introduction	283
9.2	Crystal Plasticity Modeling of Slip and Twinning	286
9.2.1	Crystal Plasticity Models	288
9.2.2	Incorporating Twinning into Crystal Plasticity Formulations	290
9.2.3	Incorporating Hardening into Crystal Plasticity Formulations	294
9.3	Introducing Lower Length Scale Statistics in Twin Modeling	300
9.3.1	The Atomic Scale	301
9.3.2	Mesoscale Statistical Characterization of Twinning	302
9.3.3	Mesoscale Statistical Modeling of Twinning	305
9.3.3.1	Stochastic Model for Twinning	306
9.3.3.2	Stress Associated with Twin Nucleation	308
9.3.3.3	Stress Associated with Twin Growth	311
9.4	Model Implementation	312
9.4.1	Comparison with Bulk Measurements	314
9.4.2	Comparison with Statistical Data from EBSD	318
9.5	The Continuum Scale	322
9.5.1	Bending Simulations of Zr Bars	324
9.6	Summary	330
	Acknowledgment	331
	References	331

- 10 Cast Magnesium Alloy Corvette Engine Cradle 337**
Haley Doude, David Oglesby, Philipp M. Gullett, Haitham El Kadiri, Bohumir Jelinek, Michael I. Baskes, Andrew Oppedal, Youssef Hammi, and Mark F. Horstemeyer
- 10.1 Introduction 337
- 10.2 Modeling Philosophy 338
- 10.3 Multiscale Continuum Microstructure-Property Internal State Variable (ISV) Model 340
- 10.4 Electronic Structures 340
- 10.5 Atomistic Simulations for Magnesium Using the Modified Embedded Atom Method (MEAM) Potential 341
- 10.5.1 MEAM Calibration for Magnesium 342
- 10.5.2 MEAM Validation for Magnesium 342
- 10.5.3 Atomistic Simulations of Mg–Al in Monotonic Loadings 343
- 10.6 Mesomechanics: Void Growth and Coalescence 347
- 10.6.1 Mesomechanical Simulation Material Model for Cylindrical and Spherical Voids 350
- 10.6.2 Mesomechanical Finite Element Cylindrical and Spherical Voids Results 350
- 10.6.3 Discussion of Cylindrical and Spherical Voids 351
- 10.7 Macroscale Modeling and Experiments 353
- 10.7.1 Plasticity-Damage Internal State Variable (ISV) Model 353
- 10.7.2 Macroscale Plasticity-Damage Internal State Variable (ISV) Model Calibration 356
- 10.7.3 Macroscale Microstructure-Property ISV Model Validation Experiments on AM60B: Notch Specimens 363
- 10.7.3.1 Finite Element Setup 365
- 10.7.3.2 ISV Model Validation Simulations with Notch Test Data 365
- 10.8 Structural-Scale Corvette Engine Cradle Analysis 366
- 10.8.1 Cradle Finite Element Model 366
- 10.8.2 Cradle Porosity Distribution Mapping 367
- 10.8.3 Structural-Scale Modeling Results 369
- 10.8.4 Corvette Engine Cradle Experiments 370
- 10.9 Summary 372
- References 373
- 11 Using an Internal State Variable (ISV)–Multistage Fatigue (MSF) Sequential Analysis for the Design of a Cast AZ91 Magnesium Alloy Front-End Automotive Component 377**
Marco Lugo, Wilburn Whittington, Youssef Hammi, Clémence Bouvard, Bin Li, David K. Francis, Paul T. Wang, and Mark F. Horstemeyer
- 11.1 Introduction 377
- 11.2 Integrated Computational Materials Engineering and Design 379

- 11.2.1 Processing–Structure–Property Relationships and Design 380
- 11.2.2 Integrated Computational Materials Engineering (ICME) and Multiscale Modeling 382
- 11.2.3 Overview of the Internal State Variable (ISV)–Multistage Fatigue (MSF) 383
- 11.3 Mechanical and Microstructure Analysis of a Cast AZ91 Mg Alloy Shock Tower 385
 - 11.3.1 Shock Tower Microstructure Characterization 386
 - 11.3.2 Shock Tower Monotonic Mechanical Behavior 387
 - 11.3.3 Fatigue Behavior of an AZ91 Mg Alloy 389
 - 11.3.3.1 Strain-life Fatigue Behavior for an AZ91 Mg Alloy 389
 - 11.3.3.2 Fractographic Analysis 391
- 11.4 A Microstructure-Sensitive Internal State Variable (ISV) Plasticity-Damage Model 391
- 11.5 Microstructure-Sensitive Multistage Fatigue (MSF) Model for an AZ91 Mg Alloy 393
 - 11.5.1 The Multistage Fatigue (MSF) Model 394
 - 11.5.1.1 Incubation Regime 394
 - 11.5.1.2 Microstructurally Small Crack (MSC) Growth Regime 395
 - 11.5.2 Calibration of the MSF Model for the AZ91 Alloy 396
- 11.6 Internal State Variable (ISV)–Multistage Fatigue (MSF) Model Finite Element Simulations 398
 - 11.6.1 Finite Element Model 398
 - 11.6.2 Shock Tower Distribution Mapping of Microstructural Properties 399
 - 11.6.3 Finite Element Simulations 401
 - 11.6.3.1 Case 1 Homogeneous Material State Calculation (FEA #1) 401
 - 11.6.3.2 Case 2 Heterogeneous Porosity Calculation (FEA #5) 401
 - 11.6.3.3 Case 3 Heterogeneous Pore Size Calculation (FEA #4) 401
 - 11.6.3.4 Case 4 Heterogeneous Material State Calculation (FEA #2) 402
 - 11.6.4 Fatigue Tests and Finite Element Results 402
- 11.7 Summary 406
 - References 407

Section III Face-Centered Cubic (FCC) Materials 411

- 12 Electronic Structures and Materials Properties Calculations of Ni and Ni-Based Superalloys 413**
 - Chelsey Z. Hargather, ShunLi Shang, and Zi-Kui Liu*
 - 12.1 Introduction 413
 - 12.2 Designing the Next Generation of Ni-Base Superalloys Using the ICME Approach 414

- 12.3 Density Functional Theory as the Basis for an ICME Approach to Ni-Base Superalloy Development 416
 - 12.3.1 Fundamental Concepts of Density Functional Theory 416
 - 12.3.2 Fundamentals of Thermodynamic Modeling (the CALPHAD Approach) 419
 - 12.4 Theoretical Background and Computational Procedure 421
 - 12.4.1 First-Principles Calculation of Elastic Constants 421
 - 12.4.2 First-Principles Calculations of Stacking Fault Energy 422
 - 12.4.3 First-Principles Calculations of Dilute Impurity Diffusion Coefficients 423
 - 12.4.4 Finite-Temperature First-Principles Calculations 426
 - 12.4.5 Computational Details as Implemented in VASP 427
 - 12.5 Ni-Base Superalloy Design using the ICME Approach 427
 - 12.5.1 Finite Temperature Thermodynamics 427
 - 12.5.1.1 Application to CALPHAD Modeling 428
 - 12.5.2 Mechanical Properties 430
 - 12.5.2.1 Elastic Constants Calculations 430
 - 12.5.2.2 Stacking Fault Energy Calculations 431
 - 12.5.3 Diffusion Coefficients 433
 - 12.5.4 Designing Ni-Base Superalloy Systems Using the ICME Approach 434
 - 12.5.4.1 CALPHAD Modeling used for Ni-Base Superalloy Design 434
 - 12.5.4.2 Using a Mechanistic Model to Predict a Relative Creep Rates in Ni-X Alloys 438
- 12.6 Conclusions and Future Directions 440
 - Acknowledgments 441
 - References 441
- 13 Nickel Powder Metal Modeling Illustrating Atomistic-Continuum Friction Laws 447**
Tonya Stone and Youssef Hammi
 - 13.1 Introduction 447
 - 13.2 ICME Modeling Methodology 447
 - 13.2.1 Compaction 447
 - 13.2.2 Macroscale Plasticity Model for Powder Metals 448
 - 13.3 Atomistic Studies 452
 - 13.3.1 Simulation Method and Setup 452
 - 13.3.2 Simulation Results and Discussion 455
 - 13.4 Summary 461
 - References 462

14	Multiscale Modeling of Pure Nickel	465
	<i>Shane A. Brauer, Imran Aslam, Andrew Bowman, Bradley Huddleston, Justin Huges, Daniel Johnson, William B. Lawrimore, Luke A. Peterson, William Shelton, and Mark F. Horstemeyer</i>	
14.1	Introduction	465
14.2	Bridge 1: Electronics to Atomistics and Bridge 4: Electronics to the Continuum	468
14.2.1	Electronics Principles Calibration Using Density Functional Theory (DFT)	470
14.2.2	Density Functional Theory Background	470
14.2.3	Upscaling Information from DFT	472
14.2.3.1	Energy–Volume	473
14.2.3.2	Elastic Moduli	473
14.2.3.3	Generalized Stacking Fault Energy (GSFE)	473
14.2.3.4	Vacancy Formation Energy	474
14.2.3.5	Surface Formation Energy	474
14.2.4	MEAM Background and Theory	474
14.2.5	Validation of Atomistic Results Using the MEAM Potential	476
14.3	Bridge 2: Atomistics to Dislocation Dynamics and Bridge 5: Atomistics to the Continuum	478
14.3.1	Upscaling MEAM/LAMMPS to Determine the Dislocation Mobility	480
14.3.2	MEAM/LAMMPS Validation and Uncertainty	481
14.4	Bridge 3: Dislocation Dynamics to Crystal Plasticity and Bridge 6: Dislocation Dynamics to the Continuum	483
14.4.1	Dislocation Dynamics Background	483
14.4.2	Crystal Plasticity Background	487
14.4.3	Crystal Plasticity Voce Hardening Equation Calibration	489
14.4.4	Crystal Plasticity Finite Element Method to Determine the Polycrystalline Stress–strain Behavior	490
14.5	Bridge 7: Crystal Plasticity to the Continuum	493
14.5.1	Macroscale Constitutive Model Calibration	499
14.6	Bridge 8: Macroscale Calibration to Structural Scale Simulations	500
14.6.1	Validation of Multiscale Methodology	503
14.6.2	Experimental and Simulation Results	504
14.7	Summary	505
	Acknowledgments	506
	References	506

Section IV Design of Materials and Structures 513

- 15 Predicting Constitutive Equations for Materials Design: A Conceptual Exposition 515**
Chung-Hyun Goh, Adam P. Dachowicz, Peter C. Collins, Janet K. Allen, and Farrokh Mistree
- 15.1 Introduction 515
- 15.2 Frame of Reference 516
- 15.3 Critical Review of the Literature 518
- 15.3.1 Constitutive Equation (CEQ) 518
- 15.3.2 Various Types of Power-Law Flow Rules in CP Algorithm 519
- 15.3.3 Comparison of FEM versus VFM 520
- 15.3.4 AI-based KDD Process 521
- 15.4 Crystal Plasticity-Based Virtual Experiment Model 522
- 15.4.1 Description of CPVEM 522
- 15.4.2 Various Types of Power-Law Flow Rules 523
- 15.5 Hierarchical Strategy for Developing a Constitutive Equation (CEQ) Expansion Model 524
- 15.5.1 Computational Model for Developing a CEQ Expansion Model 524
- 15.5.1.1 CPVEM for Predicting CEQ Patterns 525
- 15.5.1.2 Identifying CEQ Patterns for TAV 526
- 15.5.1.3 Virtual Fields Method (VFM) Model for Predicting Material Properties for New Ti-Al-X (TAX) Materials 527
- 15.5.2 Big Data Control Based on Ontology Integration 528
- 15.6 Closing Remarks 531
- Nomenclature 533
- Acknowledgments 534
- References 534
- 16 A Computational Method for the Design of Materials Accounting for the Process–Structure–Property–Performance (PSPP) Relationship 539**
Chung-Hyun Goh, Adam P. Dachowicz, Janet K. Allen, and Farrokh Mistree
- 16.1 Introduction 539
- 16.2 Frame of Reference 540
- 16.3 Integrated Multiscale Robust Design (IMRD) 542
- 16.4 Roll Pass Design 544
- 16.4.1 Roll Pass Sequence and Design Parameters 545
- 16.4.2 Flow Stress Prediction Model 548
- 16.4.3 Wear Coefficient 549
- 16.5 Microstructure Evolution Model 549
- 16.5.1 Recrystallization 550

16.5.2	Austenite Grain Size (AGS) Prediction	551
16.5.3	Ferrite Grain Size (FGS) Prediction	554
16.6	Exploring the Feasible Solution Space	555
16.6.1	Developing Roll Pass Design and The Analysis and FE Models	556
16.6.2	Developing Modules and Their Corresponding Model Descriptions	557
16.6.2.1	Module 1. AGS Prediction Model (f1)	557
16.6.2.2	Module 2. FGS Prediction Model (f2)	557
16.6.2.3	Module 3. Structure–Property Correlation	557
16.6.2.4	Module 4. Property–Performance Correlation	558
16.6.3	IMRD Step 1 in Figure 16.8: Deductive Exploration	559
16.6.4	IMRD Step 2 in Figure 16.8: Inductive Exploration	560
16.6.5	IMRD Step 3 in Figure 16.8: Trade-offs among Competing Goals	562
16.6.6	Exploration of Solution Space	562
16.7	Results and Discussion	563
16.8	Closing Remarks	568
	Acknowledgments	569
	Nomenclature	569
	References	571

Section V Education 573

17	An Engineering Virtual Organization for CyberDesign (EVOCD): A Cyberinfrastructure for Integrated Computational Materials Engineering (ICME)	575
	<i>Tomasz Haupt, Nitin Sukhija, and Mark F. Horstemeyer</i>	
17.1	Introduction	575
17.2	Engineering Virtual Organization for CyberDesign	578
17.3	Functionality of EVOCD	580
17.3.1	Knowledge Management: Wiki	580
17.3.2	Repository of Codes	582
17.3.3	Repository of Data	583
17.3.4	Online Model Calibration Tools	585
17.3.4.1	DMGfit	588
17.3.4.2	MultiState Fatigue (MSF)	591
17.3.4.3	Modified Embedded Atom Method (MEAM) Parameter Calibration (MPC)	593
17.4	Protection of Intellectual Property	595
17.5	Cyberinfrastructure for EVOCD	598
17.5.1	User Interface	598
17.5.2	EVOCD Services	600

- 17.5.3 Service Integration 600
- 17.6 Conclusions 601
- References 601

18 Integrated Computational Materials Engineering (ICME) Pedagogy 605

Nitin Sukhija, Tomasz Haupt, and Mark F. Horstemeyer

- 18.1 Introduction 605
- 18.2 Methodology 608
- 18.3 Course Curriculum 610
 - 18.3.1 ICME for Design 611
 - 18.3.2 Presentation and Team Formation 613
 - 18.3.3 ICME Cyberinfrastructure and Basic Skills 613
 - 18.3.4 Bridging Length Scales 614
 - 18.3.4.1 Quantum Methods 614
 - 18.3.4.2 Atomistic Methods 615
 - 18.3.4.3 Dislocation Dynamics Methods 617
 - 18.3.4.4 Crystal Plasticity 618
 - 18.3.4.5 Macroscale Continuum Modeling 619
 - 18.3.5 ICME Wiki Contributions 621
 - 18.3.6 Grading and Evaluation 622
- 18.4 Assessment 623
- 18.5 Benefits or Relevance of the Learning Methodology 628
- 18.6 Conclusions and Future Directions 629
 - Acknowledgments 630
 - References 630

19 Summary 633

Mark F. Horstemeyer

- 19.1 Introduction 633
- 19.2 Chapter 1 ICME Definition: Takeaway Point 633
- 19.3 Chapter 2: Takeaway Point 634
- 19.4 Chapter 3: Takeaway Point 634
- 19.5 Chapter 4: Takeaway Point 634
- 19.6 Chapter 5: Takeaway Point 634
- 19.7 Chapter 6: Takeaway Point 634
- 19.8 Chapter 7: Takeaway Point 634
- 19.9 Chapter 8: Takeaway Point 635
- 19.10 Chapter 9: Takeaway Point 635
- 19.11 Chapter 10: Takeaway Point 635
- 19.12 Chapter 11: Takeaway Point 635
- 19.13 Chapter 12: Takeaway Point 635
- 19.14 Chapter 13: Takeaway Point 635

19.15	Chapter 14: Takeaway Point	636
19.16	Chapter 15: Takeaway Point	636
19.17	Chapter 16: Takeaway Point	636
19.18	Chapter 17: Takeaway Point	636
19.19	Chapter 18: Takeaway Point	636
19.20	ICME Future	637
19.20.1	ICME Future: Metals	637
19.20.2	ICME Future: Non-Metals	637
19.20.2.1	Polymers	637
19.20.2.2	Ceramics	639
19.20.2.3	Concrete	641
19.20.2.4	Biological Materials	641
19.20.2.5	Earth Materials	643
19.20.2.6	Space Materials	644
19.21	Summary	644
	References	645

Index	647
--------------	-----

List of Contributors

Janet K. Allen

Systems Realization Laboratory
@ OU
University of Oklahoma
Norman, OK
USA

P. G. Allison

Department of Mechanical
Engineering
University of Alabama
Tuscaloosa, AL
USA

Raymundo Arroyave

Department of Materials Science and
Engineering
Texas A&M University
College Station, TX
USA

Ebrahim Asadi

Department of Mechanical
Engineering
University of Memphis
Memphis, TN
USA

Imran Aslam

Center for Advanced Vehicular
Systems (CAVS)
Starkville, MS
USA

and

Department of Mechanical
Engineering
Mississippi State University
Mississippi State, MS
USA

Michael I. Baskes

Department of Aerospace
Engineering
Mississippi State University
Mississippi State, MS
USA

and

Center for Advanced Vehicular
Systems (CAVS)
Starkville, MS
USA

Corbett C. Battaile

Department of Computational
Materials and Data Science
Sandia National Laboratories
Albuquerque, NM
USA

Irene J. Beyerlein

Theoretical Division
Los Alamos National Laboratory
Los Alamos, NM
USA

and

Department of Mechanical
Engineering, Department of
Materials
University of California
Santa Barbara, CA
USA

Clémence Bouvard

Center for Advanced Vehicular
Systems (CAVS)
Starkville, MS
USA

Andrew Bowman

Center for Advanced Vehicular
Systems (CAVS)
Starkville, MS
USA

and

Department of Mechanical
Engineering
Mississippi State University
Mississippi State, MS
USA

Shane A. Brauer

Center for Advanced Vehicular
Systems (CAVS)
Starkville, MS
USA

and

Department of Mechanical
Engineering
Mississippi State University
Mississippi State, MS
USA

Heecheen E. Cho

Center for Advanced Vehicular
Systems (CAVS)
Starkville, MS
USA

Peter C. Collins

Department of Materials Science and
Engineering
Iowa State University
Ames, IA
USA

Adam P. Dachowicz

Systems Realization Laboratory
@ OU
University of Oklahoma
Norman, OK
USA

and

School of Mechanical Engineering
Purdue University
West Lafayette, IN
USA

Haley Doude

Center for Advanced Vehicular
Systems (CAVS)
Starkville, MS
USA

B. Lynn Ferguson

DANTE Solutions, Inc.
Cleveland, Ohio
USA

David K. Francis

Center for Advanced Vehicular
Systems (CAVS)
Starkville, MS
USA

Chung H. Goh

Systems Realization Laboratory
@ OU
University of Oklahoma
Norman, OK
USA

and

Department of Mechanical
Engineering
University of Texas at Tyler
Tyler, TX
USA

Philipp M. Gullett

Department of Civil Engineering
Mississippi State University
Starkville, MS
USA

Youssef Hammi

Center for Advanced Vehicular
Systems (CAVS)
Starkville, MS
USA

Chelsey Z. Hargather

Department of Materials Engineering
New Mexico Institute of Mining and
Technology
Socorro, NM
USA

and

Department of Materials Science and
Engineering
Pennsylvania State University
University Park, PA
USA

Tomasz Haupt

Center of Advanced Vehicular
Systems (CAVS)
Mississippi State University
Starkville, MS
USA

Mark F. Horstemeyer

Center for Advanced Vehicular
Systems (CAVS)
Starkville, MS
USA

and

Department of Mechanical
Engineering
Mississippi State University
Mississippi State, MS
USA

Jeff Houze

Department of Physics and
Astronomy
Mississippi State University
Mississippi State, MS
USA

Bradley Huddleston

Center for Advanced Vehicular
Systems (CAVS)
Starkville, MS
USA

and

Department of Mechanical
Engineering
Mississippi State University
Mississippi State, MS
USA

Justin Huges

Center for Advanced Vehicular
Systems (CAVS)
Starkville, MS
USA

and

Department of Mechanical
Engineering
Mississippi State University
Mississippi State, MS
USA

Bohumir Jelinek

Center for Advanced Vehicular
Systems (CAVS)
Starkville, MS
USA

Daniel Johnson

Center for Advanced Vehicular
Systems (CAVS)
Starkville, MS
USA

and

Department of Mechanical
Engineering
Mississippi State University
Mississippi State, MS
USA

Haitham El Kadiri

Department of Mechanical
Engineering
Mississippi State University
Mississippi State, MS
USA

Seong-Gon Kim

Department of Physics and
Astronomy
Mississippi State University
Mississippi State, MS
USA

Sungho Kim

Department of Physics and
Astronomy
Mississippi State University
Mississippi State, MS
USA

William B. Lawrimore

Center for Advanced Vehicular
Systems (CAVS)
Starkville, MS
USA

and

Department of Mechanical
Engineering
Mississippi State University
Mississippi State, MS
USA

Bin Li

Ford Motor Company
Dearborn, São Paulo
Brazil

Zhichao (Charlie) Li

DANTE Solutions, Inc.
Cleveland, OH
USA

Hojun Lim

Department of Computational
Materials and Data Science
Sandia National Laboratories
Albuquerque, NM
USA

Zi-Kui Liu

Department of Materials Science and
Engineering
Pennsylvania State University
University Park, PA
USA

Laalitha S. I. Liyanage

Department of Physics and
Astronomy
Mississippi State University
Mississippi State, MS
USA

Marco Lugo

Department of Mechanical
Engineering
University of Texas at Permian-Basin
Odessa, TX
USA

Yuxiong Mao

Predictive Design Technologies
Starkville, MS
USA

Rodney J. McCabe

Materials Science and Technology
Division
Los Alamos National Laboratory
Los Alamos, NM
USA

Farrokh Mistree

Systems Realization Laboratory
@ OU
University of Oklahoma
Norman, OK
USA

David Oglesby

Paccar Engine Company
Starkville, MS
USA

Andrew Oppedal

Center for Advanced Vehicular
Systems (CAVS)
Starkville, MS
USA

Luke A. Peterson

Center for Advanced Vehicular
Systems (CAVS)
Starkville, MS
USA

and

Department of Mechanical
Engineering
Mississippi State University
Mississippi State, MS
USA

Satyam Sahay

John Deere Technology Center India
Tower XIV
Cybercity, Magarpatta City
Pune
India

ShunLi Shang

Department of Materials Science and
Engineering
Pennsylvania State University
University Park, PA
USA

William Shelton

Department of Chemical Engineering
Louisiana State University
Baton Rouge, LA
USA

Tonya Stone

Center for Advanced Vehicular
Systems (CAVS)
Starkville, MS
USA

and

Department of Mechanical
Engineering
Mississippi State University
Mississippi State, MS,
USA

Nitin Sukhija

Department of Computer Science
Slippery Rock University of
Pennsylvania
Slippery Rock, PA
USA

Ken Sullivan

Center for Advanced Vehicular
Systems (CAVS)
Starkville, MS
USA

Carlos N. Tomé

Materials Science and Technology
Division
Los Alamos National Laboratory
Los Alamos, NM
USA

Mark A. Tschopp

Army Research Laboratory (ARL)
Weapons & Materials Research
Directorate, Lightweight & Specialty
Metals Branch
Aberdeen Proving Ground
Adelphi, MD
USA

L. Arias Tucker

Los Alamos National Laboratory
Los Alamos, NM
USA

Jian Wang

Materials Science and Technology
Division
Los Alamos National Laboratory
Los Alamos, NM
USA

and

Department of Mechanical &
Materials Engineering
University of Nebraska-Lincoln
Lincoln, NE
USA

Paul T. Wang

Center for Advanced Vehicular
Systems (CAVS)
Starkville, MS
USA

William Yi Wang

Department of Materials Science and
Engineering
Pennsylvania State University
University Park, PA
USA

Christopher R. Weinberger

Department of Mechanical
Engineering
Colorado State University
Fort Collins, CO
USA

Wilburn Whittington

Center for Advanced Vehicular
Systems (CAVS)
Starkville, MS
USA

John Wilbanks

Plymouth Tube Company
Eupora, MS
USA

Mohsen Asle Zaeem

Department of Materials Science and
Engineering
Missouri University of Science and
Technology
Rolla, MI
USA

Robert Zelinka

Plymouth Tube Company
Eupora, MS
USA

Bi-Cheng Zhou

Department of Materials Science and
Engineering
Pennsylvania State University
University Park, PA
USA

Foreword

My book review on “*ICME for Metals* by Mark F. Horstemeyer” was published in the *Journal of Materials and Manufacturing Processes*. In this review, I had critiqued on two gaps seen in this first book on ICME; first, the inability to clear confusion on what exactly ICME is and second, lack of direction for industrial application of ICME. Soon after the publication of this review, I received an email from Professor Horstemeyer on accepting these gaps. He also committed to close these gaps through a second book on ICME that would majorly focus on industrial applications. Considering that Professor Mark F. Horstemeyer is one of the most prolific authors of our generation in the area of multiscale modeling in materials engineering, this email was one of the most humbling experiences for me along with a role-model behavior witnessed in handling critique toward our technical contributions.

True to his commitment, the second book on “*ICME: Industrial Applications*” focuses entirely on removing the mist from the fuzzy area of ICME and provides step-by-step guidance on its industrial application. The first chapter intriguingly starts from “What ICME is Not” to stop any modeling and simulation work in the broad area of materials engineering being presented in the garb of ICME. Furthermore, it provides necessary conditions to qualify a work as ICME along with its current industrial status. In the initial chapters, the framework for vertical bridging between electronic and atomic length scales have been revisited with example from one of the most significant industrial materials, that is, iron–carbon alloys. However, the real intent of making this book a ready reckoner on ICME for industrial users is evident in chapters on heat treatment and powder metallurgy. For example, the chapter on heat treatment and fatigue of a carburized and quench hardened steel part not only provides a modeling framework but also gives prescriptive step-by-step guidance on the experiments needed for validation of the modeling framework. The importance of experimental validation for a successful industrial realization of any modeling framework is well highlighted in this chapter. Likewise, the nuances of horizontal bridging between compaction and sintering simulations have been well described in the powder metallurgy chapter along with a very detailed

flow chart for construction on master sintering curve. These details make this book a one-stop source for thoroughly understanding and implementing the ICME approach in an industrial scenario. The chapter on internal state variable approach with use case on cast magnesium cradle for automotive application was another good refresher on the core concept of ICME having simultaneous optimization of design, manufacturing, and material considerations. This chapter also provides practical example of how prediction of failure location can be misleading without simultaneous consideration of defect location as well as peak stress location.

I strongly recommend this book to industry practitioners in order to get an illustrative but deeper insight in the exciting and evolving field of ICME. This book is intended for industrial realization and value creation through optimal design, accelerated product development, and reduced cost. Furthermore, this book also provides a good example of much needed graduate level books with industrial perspective, which would bridge the ever-growing gap between academic research and industrial realization.

Satyam Sahay, PhD
John Deere Fellow – Materials Engineering
Fellow of ASM International and Indian Institute of Metals
John Deere Technology Center India, Pune, India

Preface

In the first book on *Integrated Computational Materials Engineering (ICME)* (Horstemeyer, 2012), I covered the basic fundamentals of multiscale modeling and history modeling that included the integration of process–structure–property–performance. I also covered the different perspectives and necessary interdisciplinary requirements for ICME to work in industry or research institutions, including those from solid mechanics, materials science, numerical methods, physics, mathematics, and design. In this book, several authors present examples of employing ICME in real engineering problems, demonstrating the bridging of information between different length scales and between different materials processing and/or in-service performance environments. In another book *Data Intensive Science* (2013), I wrote about “Materials of the Future: From Business Suits to Space Suits,” basically how ICME could affect the future of materials generation in the context of President Obama’s Material Genome Initiative announced on June 24, 2011, but in the context of so-called “Big Data.”

After the first book on ICME (Horstemeyer, 2012), different documents came out that helped to bring momentum to the community. The Minerals, Metals, and Materials Society (TMS) sponsored a report (Allison *et al.*, 2012) that very nicely laid out practical steps for industry to employ ICME methodologies. The encouragement is to change the paradigm in industry to embrace ICME methodologies in order to make parts optimized by reducing time, reducing cost, saving weight, and increasing in-service life cycle performance. As such, this book is an endeavor to illustrate some ICME methodologies for practical engineering case studies. The community has a long way to go, but hopefully these cases presented herein will demonstrate to the reader that the risk involved in moving toward an ICME paradigm is not really that large. In fact, the benefits will typically outweigh the risk.

These case studies will also help clarify what ICME really is. In the community there are some misunderstandings that need clarification as ICME continues to grow in influence. In the first ICME book (Horstemeyer, 2012), I gave a history of the different disciplines (materials science, applied mechanics, numerical

methods, physics, mathematics, and design) that have come together to form the notion of ICME. There have been two independent ICME conferences to date and several symposia sponsored by TMS recently. These events indicate that ICME is growing in momentum; however, since practical examples have not been forthcoming in rampant numbers, this book is warranted.

Besides the introduction, there are three main sections in the book. The first section addresses what is called “Horizontal ICME” addressing case studies that connected the process–structure–property–performance sequence. The materials processing examples here are related to casting, rolling, compaction/sintering of powder metals, heat treating, and tube processing. The second section addresses what is called “Vertical ICME,” which is related to multiscale materials modeling. Although there is a bit of multiscale modeling in the first section examples, the case studies in the second section still quantify structure–property relationships but are focused on different length scale bridging. The third section is related to Education. The ICME course has been taught three times at Mississippi State University (MSU) for in class students and for distance learning students. The last course taught in 2014 was taught to not only MSU students and random distance students but also to graduate students at Louisiana State University (LSU) with a co-instructor being Dr. Bill Shelton. For the reader, the course is available to anyone via a distance learning venue, and the book on for the course is the first ICME (Horstemeyer, 2012) book.

I want to thank the different authors and colleagues who have contributed to this particular book. These authors are at the forefront of ICME today, so their insights and examples can help the community at-large to understand and appreciate much more the different aspects of ICME. Also, I certainly do not want to offend some who have used ICME concepts in either Vertical ICME or Horizontal ICME projects and are not mentioned in this book. If you keep using the ICME concepts, your reward will be much greater than having a chapter in this book, for sure.

I would also like to thank by dear wife, Barbara, who has been supporting me so much in all of my work endeavors. My administrative assistant at work is Rose Mary Dill who, if you have met, will always be remembered by her smile and her encouraging words. If you have not met Rose Mary, it is too bad, because she is someone special. She has covered my errors, softened my harshness, and has added excellence to all my work. I must also recognize all of my students, post-doctoral researchers, and research staff at CAVS at MSU. In particular, I wanted to thank Justin Hughes, Shane Brauer, and Kyle Johnson for their helping with editing of the text. Without these folks all buying into the ICME message and doing the work, my success would be minimized. I have truly stood on the shoulders of giants as Isaac Newton once stated. The giants in my life are those I just mentioned.

Finally, I would like to challenge the community at-large to be willing to try ICME concepts in their businesses. The ICME return-on-investment (ROI) is usually between three and seven times in my experiences, when these ROI numbers were determined from immediate returns. The longer term returns are not included in the numbers that I have shared, so they are probably larger. I suspect that others have ICME examples that have a greater ROI than seven times. Regardless, the diffusion of this technology will grow as more successes are realized as demonstrated in this book.

Mark F. Horstemeyer, PhD
Giles Distinguished Professor and CAVS Chair Professor
Fellows in ASME, ASM, SAE, and AAAS
Mechanical Engineering
Mississippi State University

1

Definition of ICME

Mark F. Horstemeyer^{1,2} and Satyam Sahay³

¹Department of Mechanical Engineering, Mississippi State University, Mississippi State, MS, USA

²Center for Advanced Vehicular Systems (CAVS), Starkville, MS, USA

³John Deere Technology Center India Tower XIV, Cybercity, Magarpatta City, Pune 411 013, India

What is ICME? As some confusion exists regarding its definition in the scientific community, deliberating on this topic is worthwhile. In fact, litigating on some of the terms needs attention so that redundancies related to other fields, pedagogical lapses in education, misunderstandings of researchers who are trying to garner funding, and minimal use of integrated computational materials engineering (ICME) in industry can be decreased. First, let us consider what is not ICME.

1.1 What ICME Is NOT

1.1.1 Adding Defects into a Mechanical Theory

ICME is not just adding material defects into a mechanical theoretical model. Nabarro (1952) placed the notion of dislocations into mechanics equations just to name a few. Hall (1951) and Petch (1953) added grain size effects to the stress state relationship. Eshelby (1957, 1959) described how to analytically place inclusions into a medium to determine the aggregate response, which was the basis for most, if not all, of the microscale and mesoscale homogenization theories that have been used today for metals, composites, and ceramics. This list is not exhaustive by any means but illustrates that adding defects into a continuum theory has been around quite a long time. As such, if ICME is “new,” then adding different scales of defects into a mechanical theory is not ICME. It is necessary for ICME but not sufficient within itself.

1.1.2 Adding Microstructures to Finite Element Analysis (FEA)

Dawson (1987) and Beaudoin *et al.* (1994) included crystalline texture into FEA under large deformations. Later, Ghosh *et al.* (1995) put different length scale microstructures into finite element meshes and solved large deformation problems. At the same time, Fish and Belsky (1995) allowed heterogeneous microstructures into a finite element formalism. Again, this list is not exhaustive just illustrative that adding microstructures into finite element analysis (FEA) existed before ICME. Hence, just adding microstructural heterogeneities is not ICME per se, but can be a part of ICME if other simulations are included beyond those of the particular microstructure sensitive FEA.

1.1.3 Comparing Modeling Results to Structure–Property Experimental Results

Frankly speaking, this topic should not be included in here because it is so clear to many; however, I have observed in symposia and large conferences on ICME, this issue arises from different researchers' presentations. Although the essence of the scientific method started before Bacon (1605), it was formalized into the fundamental steps that we all know today: (1) Make an observation; (2) form a hypothesis; (3) design and conduct an experiment to falsify the hypothesis; if the hypothesis is not falsified, it becomes a theory; and (4) design more experiments to validate the theory after which the theory becomes a law when not invalidated. The most basic form of the scientific method is what is presented when a researcher compares modeling (hypothesis) to structure–property relationships (experiments), not ICME. Applying the scientific method to ICME is indeed important and is a necessary requirement for ICME to be realized; however, the scientific method is not ICME just a necessary part of it.

1.1.4 Computational Materials

Researchers in computational materials started much earlier than ICME. With the advent of large-scale computers (Cray for example) in the 1980s, atomistic simulations were tractable in trying to understand mechanisms related to mechanical properties. Daw and Baskes (1984) embedded atom method (EAM) and Baskes (1992) modified embedded atom method (MEAM) potentials allowed for the burgeoning of computational materials to proliferate at the time. At the same time, electronics structures calculations (a length scale lower than that in Baskes *et al.* work) were employing large-scale computing environments to provide understanding of energies and some defects in materials. Yip's (2005) fairly recent Handbook of Materials Modeling is an excellent resource in the state-of-the-art computational materials methods.

Yip and his coauthors (2005) broke down the computational materials aspects into electronic-scale calculations, atomistic-scale calculations, mesoscale calculations, and continuum-scale calculations focusing on areas such as rate effects, crystal defects, microstructures, fluids, and polymers. This book represents the truest sense of computational materials, but it is not ICME. Why? Because nothing is integrated and no engineering exists in computational materials; computational materials is typically limited to science (the discovery of what exists). As such, computational materials is a necessary ingredient to ICME but not sufficient to represent ICME.

1.1.5 Design Materials for Manufacturing (Process–Structure–Property Relationships)

ICME is not just designing materials using process–structure–property relationships. Designing materials for manufacturing and in-service life initiated in the 1980s when computer aided design (CAD) and computer aided manufacturing (CAM) were first exploded on the scene. Terms such as “Virtual Manufacturing,” “Simulation-Based Design,” “Virtual Prototyping” have become common vernacular now in the design industry. Granted, most of these emphases did not focus on the “structure” part of the process–structure–property relationships, but the notion and the attempt were made mainly from the mechanical engineering discipline. Mathur and Dawson (1987) correlated the process–structure–property relations of drawing with the porosity evolution, which, in turn, gave mechanical properties. Shortly after, Mathur and Dawson (1989) embedded a crystal plasticity theory into finite element simulations to capture the texture evolution in forming processes, which, in turn, yielded different mechanical properties than when the material was initialized. These examples typify process–structure–property computing and certainly could be considered computational materials but not really ICME.

1.1.6 Simulation through the Process Chain

In many of the ICME workshops and conferences, simulation across the process chain has been presented as an ICME example. For example, simulations of several unit processing of a steel mill (e.g., LD furnace, ladle refining, tundish, continuous casting) are simulated by linking the output of the preceding step to the input of next step. These modeling studies are extremely complex and very important in understanding the interactions and impact of different stages on the final product quality. Nevertheless, these are not valid ICME examples as such cases have limited focus and integration on the design aspect of ICME as well as misses on the life-cycle analysis. Furthermore, these examples have existed in literature before the ICME framework was created.

1.2 What ICME Is

1.2.1 Background

Olson (1998, 2000) was one of the first from the materials science community who articulated what researchers were trying to realize in the process–structure–property relationships. The National Academy of Engineering (NAE) (2008) and The Minerals, Metals, and Materials Society (TMS) reports (2012), although very helpful and useful, picked up on the process–structure–property relationships from that of Olson (1998, 2000). The two reports did indeed pick up the “Integration,” “Computational Materials,” and “Engineering” aspects, but they left out the associated mechanics aspects of the life-cycle performance. Hence, the process–structure–property relationships need to be really process–structure–property–performance relationships as delineated in Horstemeyer (2012, 2013). Including “performance” in the paradigm is not something new and has been the focal point of the mechanics communities for years, long before ICME came into vogue. Even Olson (1998, 2000) and the NAE and TMS reports make a mention of the mechanics aspects, but they leave it out of the “inner circle” of information. However, to realize the goals mentioned in the NAE and TMS reports, the performance evaluation along with multiobjective optimization that includes uncertainty analysis is required in true ICME fashion. Figure 1.1 illustrates the fact that the performance requirements need to be thought of first, before starting the ICME simulations (i.e., the notion of starting with the end in mind).

All of these aforementioned ideas by themselves are just *necessary conditions but not sufficient* for ICME. It is the “Integration” and the “Engineering” of all of the previous points that make ICME true ICME. Some have claimed that ICME is a misnomer:

1. It could be called ICMSE, because “science” needs to be included. Science is the discovery of what exists, and certainly discovery of new structure–property relations at different length scales will be crucial to engineer new materials and structures.
2. It could also be called ICMME, because “mechanics” needs to be in the name just as much as the other terms. Again, this is true to an extent.
3. It could also be called ICM³E, because “mechanics” and “manufacturing” should be included. Again, this is true.

One could unquestionably argue that ICME is probably not the best acronym to describe what is really going on; in any case, we will stick to it since any term that is used would include imperfections. However, we will more clearly define ICME through a series of case studies focused on bridging between length

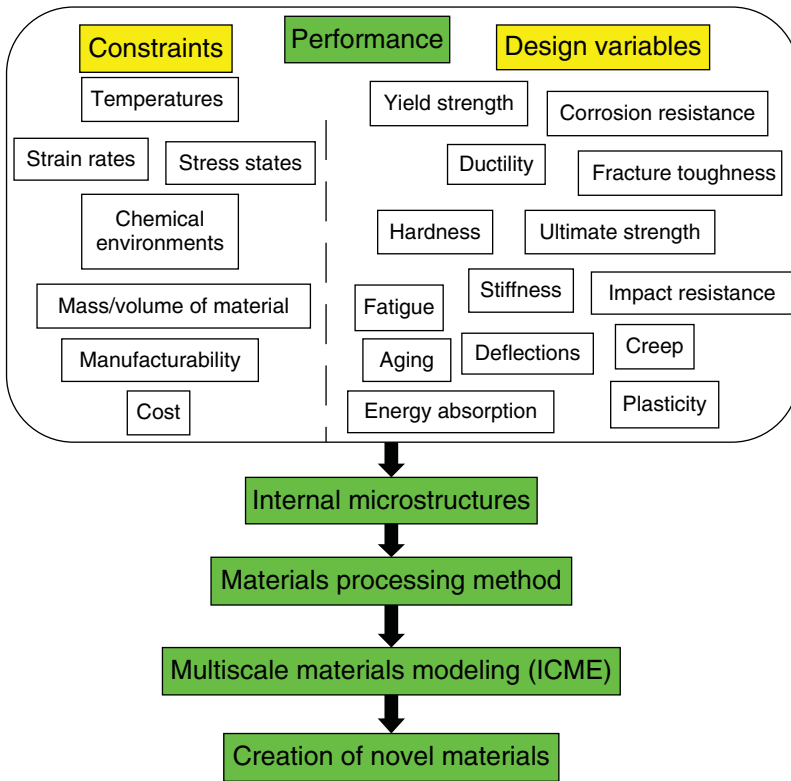


Figure 1.1 Schematic illustration of solving the inverse problem where the performance requirements are examined first and then the creation of new materials is backed out at the end (Horstemeyer, 2012).

scales (Vertical ICME) or bridging between steps in processing or the in-service performance life cycle (Horizontal ICME).

1.2.2 ICME Definition

ICME is the bridging of information from *two or more experimentally validated models or simulation codes* in which structure–property information passes from one code to another: (1) for “Horizontal ICME” the simulation codes connect the sequential materials processes with their associated multiscale structures to their mechanical properties that can be used in the performance life-cycle evaluation so the heterogeneities of the multiscale structures and history are embedded into the simulation codes; (2) “Vertical ICME” the simulation codes connect the multiple length scale cause-effect relationships that are heterogeneous in nature and embedded into the simulation codes,

or (3) for a “Hybrid ICME” in which both Horizontal ICME and Vertical ICME are integrated.

With this definition, one can allow discrete defects in a mechanical theory, include microstructures into a finite element code, compare modeling results to structure–property experimental results, require computational materials approaches, admit applied mechanics into the heart of the modeling, and include the process–structure–property relationships.

The case studies in this book have two different types of information passing in which bridging is required so that information can be passed with necessary and sufficient conditions. Figure 1.2 illustrates the connection of information passage via multiple length scales and via the processing and performance life cycle. The horizontal information passage (Horizontal ICME) is different than the vertical multiscale modeling information passage (Vertical ICME). Hence, the figure shows both the “Vertical ICME” and “Horizontal ICME” for one case study that was discussed in Horstemeyer and Wang (2003).

Although Figure 1.2 shows five different length scales from the nanoscale to the structural scale, ICME does not need to have that many length

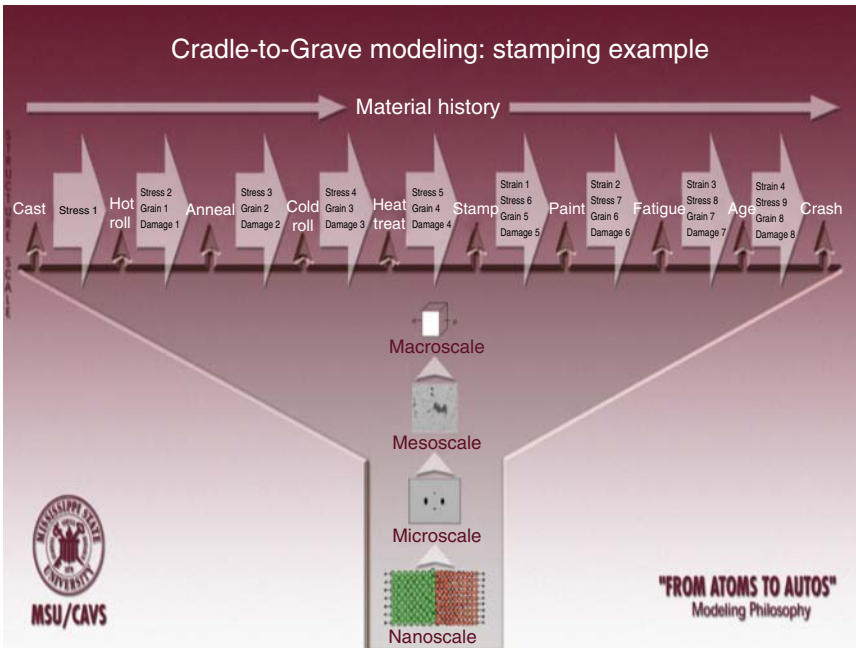


Figure 1.2 In order to capture the Cradle-to-Grave history, robust models must be able to capture various manufacturing and in-service design scenarios (Horstemeyer and Wang, 2003). This example shows that integration of information passage is required for both the “Horizontal ICME” sequence and the “Vertical ICME” sequence. (See color plate section for the color representation of this figure.)

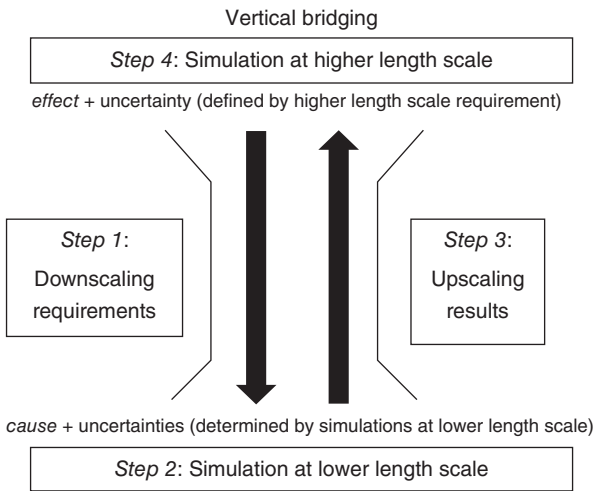


Figure 1.3 “Vertical ICME” bridging between two different length scales of simulations showing the sequential steps of the ICME methodology.

scales involved. In fact, only two different length scale simulations in which information is passed can be considered “Vertical ICME.” Figure 1.3 shows the steps involved in the vertical integration of two different length scales.

Step 1: Downscaling occurs first in which the “effects” or the information that is needed at the higher length scale is defined.

Step 2: Once the effects are defined, lower length scale modeling and simulations are conducted in order to garner those effects as simulation results. At this point, experiments can be used to calibrate and validate the lower length scale simulation results to ensure that “good” information is passed back up to the higher length scale simulation.

Step 3: Upscaling the results from the lower length scale simulations can be straightforward if the foreordained downscaling requirements demanded specific data for the higher length scale model. If the lower length scale results are more general and do not directly fit into the higher length scale model, then engineering judgment is needed to help use the lower length scale results to calibrate the higher length scale model. Calibrating the higher length scale model is the goal of upscaling. Sometimes, experimental data can be used to calibrate a model but if the experimental data is missing, then the lower length scale simulation results can help calibrate the model.

Step 4: Once model calibration is completed, the higher length scale can then be validated with an experiment or set of experiments performed at that length scale. Once validated, the model can be used to predict the behavior for the next length scale higher or for the final results, whichever is needed.

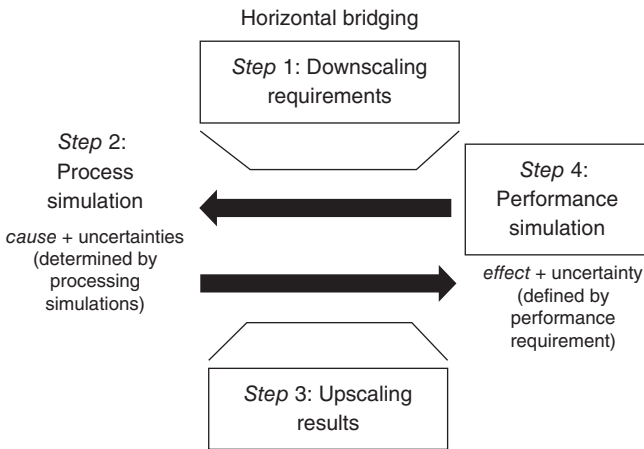


Figure 1.4 “Horizontal ICME” bridging between two different steps in the process–performance sequence of simulations showing the sequential steps of the ICME methodology.

The “Horizontal ICME” case studies in this book did not focus on the vertical bridging of information but on the horizontal bridging. The downscaling (downstream is used in manufacturing processing) and upscaling methodologies are similar to the vertical methodology. Figure 1.4 shows the example of the “Horizontal ICME.”

- Step 1:* Downscaling occurs first in which the “effects” or the engineering design requirements are first defined and passed backward to the previous step in the process (used as downscaling here).
- Step 2:* Once the engineering requirements are defined, modeling and simulations in the previous step of the process–structure–property–performance sequence are conducted. At this point, experiments can be used to calibrate and validate the simulation results to ensure that “good” information is passed through to the next sequential simulation.
- Step 3:* Upscaling the results from the previous simulations is simply to help calibrate the model for the next simulation down either the processing steps or the life-cycle performance steps. Initializing the simulations with the previous information is key to capturing the history effects.
- Step 4:* Once model calibration is completed, the next step in the simulation sequence can then be used to predict the behavior either in the next step in the process or for the final results, whichever is needed.

1.2.3 Uncertainty

Another notion that is presented in each of these case studies is the idea of uncertainty. Different types of uncertainties can exist in an analysis. A simple

Schematic of verification and validation of a simulation

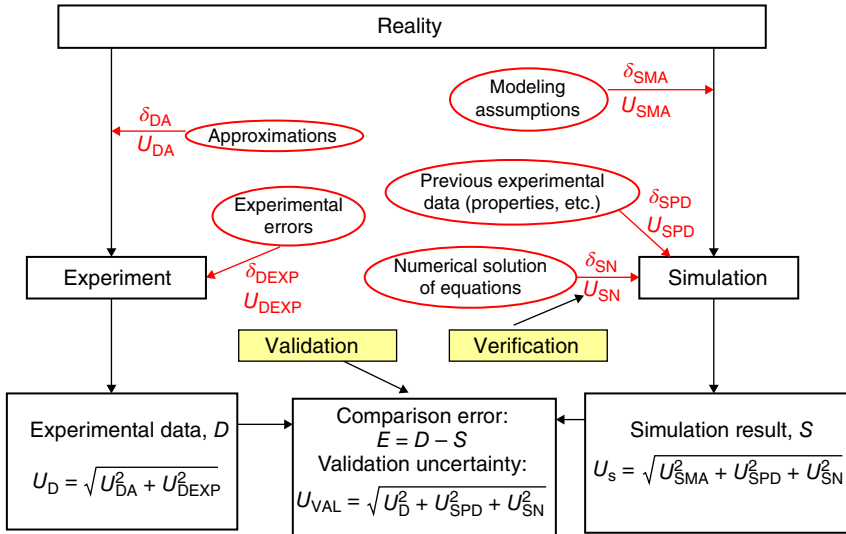


Figure 1.5 Uncertainty analysis is useful in bringing robustness to an industrial usage of ICME. Here, the modeling and simulations need to be validated by examination of an uncertainty analysis.

way to think about uncertainty is that if one can get 10,000 results from testing, then the extent of the *errors* will encompass that of the *uncertainty* of the results. Essentially, the *errors* are the *uncertainty*. However, we typically never run 10,000 tensile tests to get one stress–strain curve; we may test 3–5 specimens and sometimes 10 at most. In the case where we conduct just a few tests, we need to conduct a formal uncertainty analysis in order to bound the results to ensure the “goodness” of the data transferred to the next higher length scale if vertical bridging is involved or to the next processing or performance step in horizontal bridging is involved. Figure 1.5 illustrates that when the uncertainty of the simulation results are less than those of the experimental results around a mean value, then “validation” is said to have occurred. Inherent within the uncertainty analysis is including experiments in which the structure–property relationships are quantified and used in that particular simulation.

1.2.4 ICME Cyberinfrastructure

Before moving on to the ICME case studies, one more notion needs to be discussed. A cyberinfrastructure has been started at <http://icme.hpc.msstate.edu>, and is described in Chapter 17 of this book in which anyone can learn the modeling and simulation codes at different length scales and garner experimental data. Furthermore, case studies can be included on the website. Figure 1.6

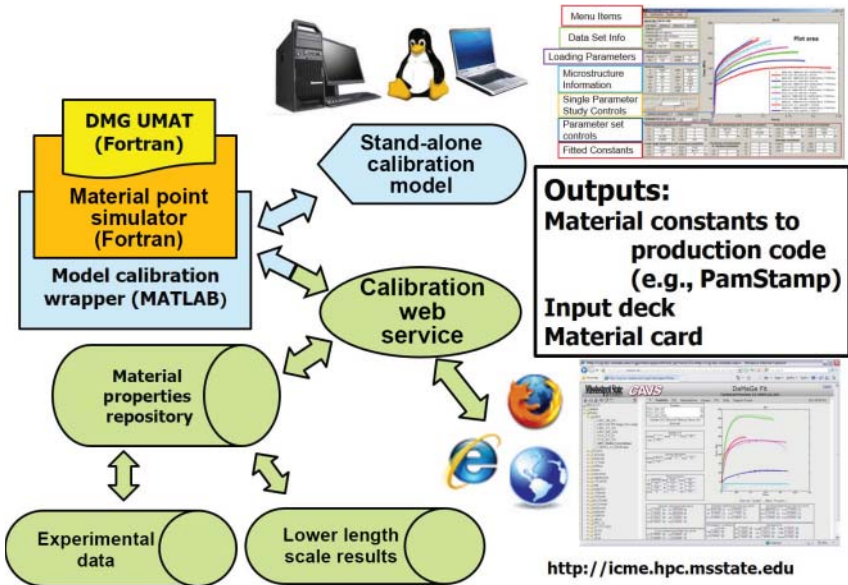


Figure 1.6 The ICME cyberinfrastructure houses repositories for models and codes, materials characterization data, experimental stress–strain data, and different calibration tools. Examples of running different codes are also included in a tutorial fashion. (See color plate section for the color representation of this figure.)

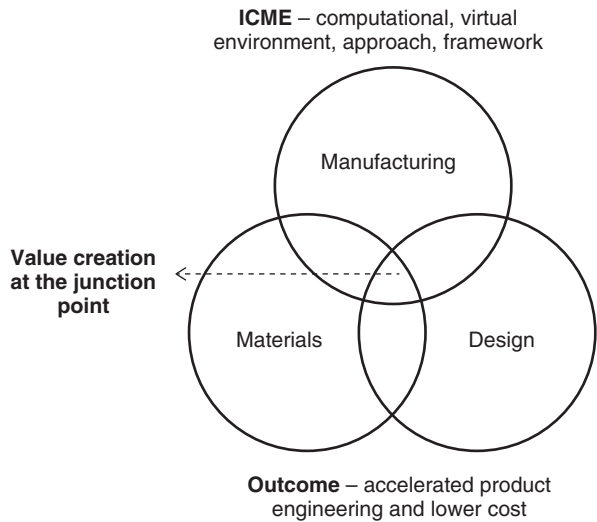
illustrates the different relationships of information that can be placed or used on the ICME cyberinfrastructure website. One final comment is that the website is WIKI-based, so anyone who requests an account from the author can use the site and add their own information, knowledge, and wisdom as well.

1.3 Industrial Perspective

There are three open questions around ICME, which puzzles most of the materials engineering leadership in industry:

- a. In simple terms, what really is ICME? Hopefully, we have answered it earlier. If not, we ask the reader to be patient and maybe the case studies will help clarify it.
- b. Can ICME mature to be transitioned to industry and deliver value? We hope to answer this question for the reader next.
- c. In the context of a specific organization, how do we identify opportunities for ICME? We hope to answer this question next as well.

Figure 1.7 ICME as the value creation at the junction point of design, materials, and manufacturing through a computational framework.



ICME is a computational framework, which integrates design, materials, and manufacturing during product development and creates value at their junction point (Figure 1.7). The value creation is an engineering realization through accelerated development cycle and/or reduced product cost.

The maturity curve of a computational technique is illustrated in Figure 1.8, where any new method evolves from a research project to a special tool, framework, design process, and hardware integration. In this progression, the ease of usage and scalability increase along with the probability of usage and value creation. A matured framework is an inflection point where the method transitions from a technology push to a business pull. In the business pull regime, the technology is matured and its ROI has been established. For example, FEA software has become an integral part of the product engineering life cycle and practically every component of a product gets virtually validated through a commercial FEA code. The method is scalable to every component of the enterprise and the value is derived from significant reduction in prototyping and physical testing of individual components. A matured framework, like six-sigma, is at the inflection point, which is scalable, yet needs special focus for their enhanced usage.

In the technology-push regime, for a special research initiative or special tool, the onus is on the researchers and technical leadership to identify appropriate use-cases and demonstrate the effectiveness and value of the methodology. Currently, ICME is in this technology-push regime, where the focus should be on maturity of methodology and creation of portfolio of use-cases demonstrating its effectiveness and value.

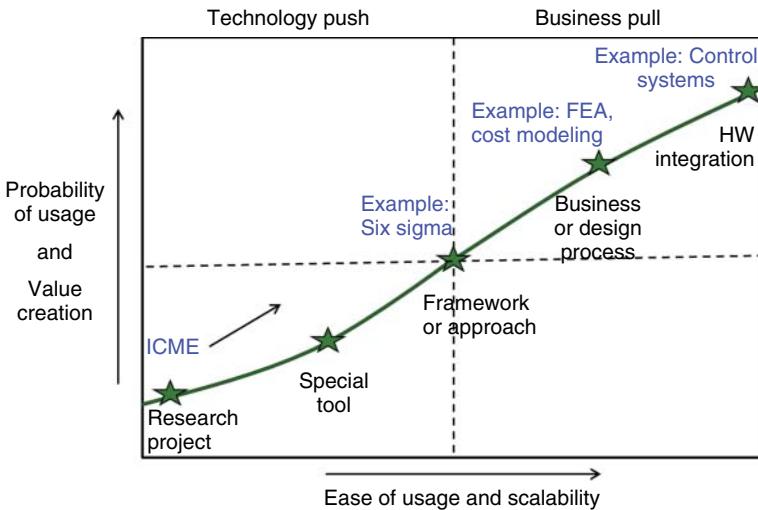


Figure 1.8 Methodology adoption curve in an industry.

During the last seven to eight years, significant enthusiasm has been centered around ICME, including several symposia and a few conferences. However, very few specific industrial case-studies have been reported in the literature. For the long term, several solutions have been envisaged, including (1) development of an integrated computational platform, which automates and enables ICME and (2) coupled simulation tools for product development, which enables design for performance, manufacturing, alloy design, cost, and sustainability. Although these long-term solutions will provide transformational platform for product engineering, several near-term opportunities are available in the ICME space.

The near-term ICME solution invariably includes bootstrapping of existing methods, tools, and techniques. The key consideration for these opportunities is to forget the legacy designs, materials, or manufacturing considerations and relook at the current product engineering cycle as a white-space opportunity. For example, consider an electronic cooling system (Figure 1.9), which is conventionally created by machining cylindrical holes as cooling pipes. Newer techniques of design optimization would enable placement of holes and their shapes for efficiency improvements. If a new manufacturing technique like additive manufacturing is adapted for making this cooling system, with current design considerations, it would primarily result in rapid prototyping. This would lead to reduction in tools and fixtures, without any significant disruption in the design. However, in order to realize the full potential of additive manufacturing, the constraint-free design should be adapted. In this paradigm, the shape of cylindrical holes can be changed to star-shaped,

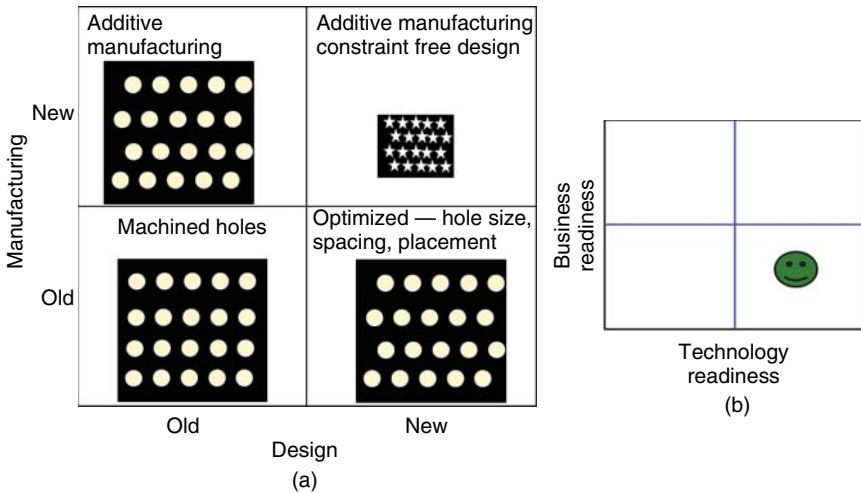


Figure 1.9 (a) Significant value creation by co-adoption of new design, materials and manufacturing techniques resulting in breakthrough products. (b) For this specific opportunity, the technology readiness level is higher and the gap is to identify business opportunities.

which are not feasible through conventional methods. Furthermore, the pipes can be interconnected for higher efficiency. Finally, the microstructure and phases can be spatially tailored, which could provide unprecedented efficiency and thereby significant reduction in the cooling system size. Recently, a few examples have been created for production of highly complex parts or part assembly providing unprecedented design simplification or high performance through additive manufacturing. The technology of additive manufacturing is mature for such specific engineering realizations of ICME, although the history modeling of the thermomechanical couplings could still use some progress. There is need for improving the business readiness (Figure 1.9) and identifying specific component usage of this particular technology.

Additive manufacturing provides significant opportunities for high-performance components having complex design, such as hydraulics valves or nozzles, which are hitherto unconceivable through traditional design and manufacturing methods. Similarly, any new technology adaption, such as lightweighting or newer joining techniques such as adhesive bonding have to be leveraged through simultaneous co-adoption of newer materials, newer manufacturing methods, and a newer design philosophy. In turn, they provide significant opportunity for the ICME framework to be leveraged in the industry.

ICME can be leveraged at multiple scales and multiple processing steps into the performance regime to efficiently design specific components and

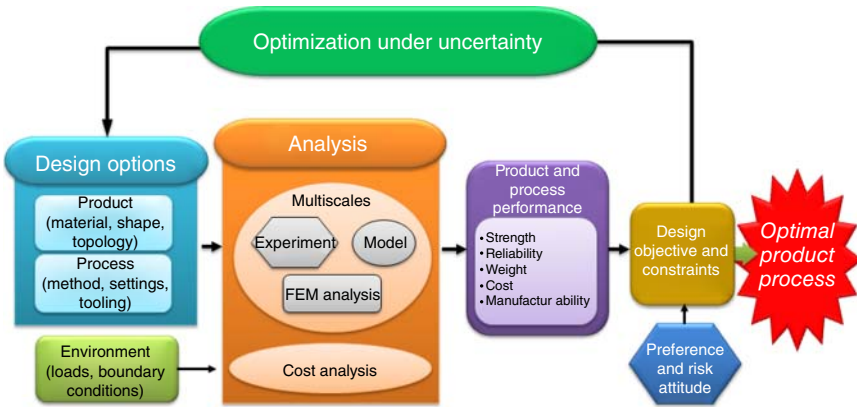


Figure 1.10 Schematic illustrating the co-adoption of multiscale models that were experimentally validated within a finite element method (FEM) coupled with a cost analysis, uncertainty analysis, and multiobjective design optimization analysis can help design new materials, new structures, and new manufacturing processes.

systems. An integrated framework for traditional materials and manufacturing has been proposed in Figure 1.10 garnered from Horstemeyer (2012), where design, processing, and product verification phases are coupled for realizing an optimal and robust component (Sahay and El-Zein, 2011; Sahay, 2014), while including uncertainties. In this framework, the design and FEA steps are coupled along with tooling and process considerations for the optimization purpose. This coupling significantly reduces the design-FEA iteration cycle as well as enables the optimal product design. Furthermore, in the ICME framework, cost and performance have been incorporated for a holistic design, and the design can be on a new material, or a new shape or even a new topology. This framework incorporates the multiscale structures (particles, inclusions, grains, etc.) and associated residual stresses from the process simulation into the product performance phase. This simple framework provides opportunities for efficient design of castings, wrought materials, powder metals, and heat-treated components.

Besides the technology readiness and business readiness, talent availability in this niche domain is the most significant challenges for adaption of ICME in industry. There is significant shortage of talent with required skill sets for this area. The functional silos of design, manufacturing, and materials engineers with their traditional experience-based expertise would be the major bottleneck in the scale-up of this technology in the industry. It is imperative to develop computational-skill-based expertise in the materials, manufacturing, and design engineering competencies. Furthermore, multifunctional teams need to be created for this special initiative, where interdisciplinary mindset

should be nurtured through specific projects in the context of organization. In general, the required competency levels as well as needed capacity for the scale-up in most of the organizations are generally low. It would require at least a decade to nurture this capability in any organization for making meaningful business impact so patience is needed to justify the investment and commitments. However, the significant pay-offs and value creation from this capability would provide speed, differentiation, and significant efficiencies in product engineering.

1.4 Summary

In summary, there are multiple near-term as well as long-term opportunities for engineering realization of ICME in the industrial setup. In the long run, co-adoption of new materials, new structures, new manufacturing techniques, and new design philosophies is required for breakthrough designs. Furthermore, a formal tool or simulation methods can be developed for automation and scale-up of ICME in the long term. In the short term, significant value can be created by incorporating the manufacturing or performance simulation prediction in the design phase along with cost modeling. This can be achieved by bootstrapping the currently available tools and techniques. In both short-term and long-term cases, the focus should be on identifying appropriate use-cases relevant to the specific industry as well as organizational context. It is imperative to develop this niche capability in an organization by putting a significant focus on competency development as well as capacity enhancement by creating a multifunctional team with interdisciplinary mindset. The high ROI and business impact would justify the organizational investments made in this emerging area.

References

- Allison, J., Cowles, B., DeLoach, J. *et al.* (2012) *Integrated Computational Materials Engineering (ICME): Implementing ICME in the Aerospace, Automotive, and Maritime Industries*, The Minerals, Metals & Materials Society, Warrendale, PA.
- Bacon, F. (1605) *The Advancement of Learning*, Book I, v, 8.
- Baskes, M.I., Modified embedded-atom potentials for cubic materials and impurities," *Physical Review B* **46**, 2727, 1992, 2727–2742.
- Beaudoin, A.J., Dawson, P.R., Mathur, K.K. *et al.* (1994) Application of polycrystal plasticity to sheet forming. *Computer Methods in Applied Mechanics and Engineering*, **117** (1–2), 49–70.

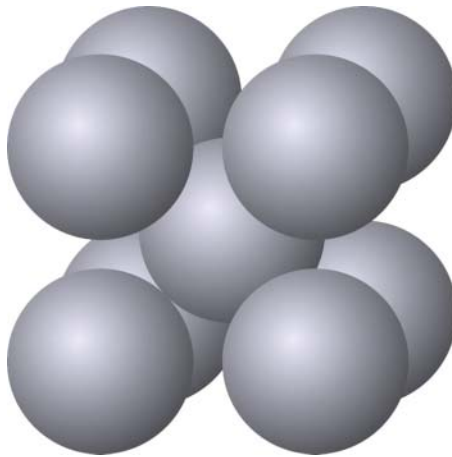
- Daw, M.S. and Baskes, M.I. (1984) The embedded-atom method: derivation and application to impurities, surfaces, and other defects in metals. *Physical Review B*, **29** (12), 6443.
- Dawson, P.R. (1987) On modeling of mechanical property changes during flat rolling of aluminum. *International Journal of Solids and Structures*, **23** (7), 947–968.
- Eshelby, J.D. (1957) The determination of the elastic field of an ellipsoidal inclusion, and related problems. *Proceedings of the Royal Society of London. Series A: Mathematical and Physical Sciences*, **241** (1226), 376–396.
- Eshelby, J.D. (1959) The elastic field outside an ellipsoidal inclusion. *Proceedings of the Royal Society of London. Series A: Mathematical and Physical Sciences*, **252** (1271), 561–569.
- Fish, J. and Belsky, V. (1995) Multi-grid method for periodic heterogeneous media. Part 2: Multiscale modeling and quality control in multidimensional case. *Computer Methods in Applied Mechanics and Engineering*, **126** (1–2), 17–38.
- Ghosh, S., Lee, K., and Moorthy, S. (1995) Multiple scale analysis of heterogeneous elastic structures using homogenization theory and Voronoi cell finite element method, *International Journal of Solids and Structures*, **32** (1), 27–62.
- Hall, E.O. (1951) The deformation and ageing of mild steel: III discussion of results. *Proceedings of the Royal Society of London Series B*, **64** (381), 747–753.
- Horstemeyer, M.F. (2012) *Integrated Computational Materials Engineering (ICME) for Metals: Using Multiscale Modeling to Invigorate Engineering Design with Science*, Wiley Press, Hoboken, NJ.
- Horstemeyer, M.F. (2013) Materials of the future: from business suits to space suits, *Data-Intensive Science*, Chapter 5, *Computational Science Series*, (eds T. Critchlow and K. Kleese van Dam), Chapman and Hall/CRC, Boca Raton, London, New York, pp. 103–120.
- Horstemeyer, M.F. and Wang, P. (2003) Cradle-to-Grave simulation-based design incorporating multiscale microstructure-property modeling: reinvigorating design with science. *Journal of Computer-Aided Materials Design*, **10**, 13–34.
- Mathur, K.K. and Dawson, P.R. (1987) On modeling damage evolution during the drawing of metals, *Mechanics of Materials*, **6** (3), 176–196.
- Mathur, K.K. and Dawson, P.R. (1989) On modeling the development of crystallographic texture in bulk forming processes. *International Journal of Plasticity*, **5** (1), 67–94.
- Nabarro, F.R.N. (1952) Mathematical theory of stationary dislocations. *Advances in Physics*, **1**, 269–394.
- NAE (2008) *Integrated Computational Materials Engineering: A Transformational Discipline for Improved Competitiveness and National Security*, NAE <https://books.google.com/books?id=JlfSnH8jI4UC&dq=Standardized+information+exchange+in+Integrated+Computational+Materials+Engineering+-wikipedia>.
- Olson, G.B. (1998) Systems design of hierarchically structured materials: advanced steels. *Journal of Computer-Aided Materials Design*, **4** (3), 143–156.

- Olson, G.B. (2000) New age of design. *Journal of Computer-Aided Materials Design*, 7, 143–144.
- Petch, N.J. (1953) The cleavage strength of polycrystals. *Journal of the Iron and Steel Institute*, 174 (1), 25–28.
- Sahay, S.S. (2014) Heat treatment of gears, in *ASM Handbook – Vol. 4D Heat Treating Iron and Steel*, pp. 204–218.
- Sahay, S.S. and El-Zein, M. (2011) Technological Vision: residual stress engineering for leaner, greener and safer design. *Surface Engineering*, 27 (2), 77–79.
- Yip, S. (2005) *Handbook of Materials Modeling*, Springer <http://www.springer.com/us/book/9781402032875>.

Section I

Body-Centered Cubic Materials

The next section includes Chapters 2–7 associated with just body-centered cubic (BCC) materials. Most of the chapters here focus on steel alloys addressing both horizontal and vertical upscaling and downscaling in the context of Integrated Computational Materials Engineering (ICME). The figure below illustrates the atom positions for a BCC metal.



Schematic of a body-centered cubic (BCC) crystal.

2

From Electrons to Atoms: Designing an Interatomic Potential for Fe–C Alloys

Laalitha S. I. Liyanage¹, Seong-Gon Kim¹, Jeff Houze¹, Sungho Kim¹, Mark A. Tschopp², Michael I. Baskes^{3,5}, and Mark F. Horstemeyer^{4,5}

¹Department of Physics and Astronomy, Mississippi State University, Mississippi, MS 39762, USA

²Army Research Laboratory (ARL), Weapons & Materials Research Directorate, Lightweight & Specialty Metals Branch, Aberdeen Proving Ground MD 21005, USA

³Department of Aerospace Engineering, Mississippi State University, Mississippi State, MS 39762, USA

⁴Department of Mechanical Engineering, Mississippi State University, Mississippi State, MS, USA

⁵Center for Advanced Vehicular Systems (CAVS), Starkville, MS, USA

2.1 Introduction

This chapter presents the case study of bridging the two lowest length scales within the Integrated Computational Materials Engineering (ICME) paradigm, namely, the electronic and atomic scales, using the case of developing an interatomic potential for Fe–C alloys. Several other chapters in this book will use the bridging of information from the electronic to the atomic scale, but they will not go into the details about the bridge as much as this chapter.

Steel alloys are the most widely used structural materials due to their abundance, all-purpose applicability, and low cost. The main carbide in steel alloys is cementite, which forms a precipitate. Cementite has a direct impact on the mechanical, structural, and thermal properties of steel. Therefore, the ability to describe and predict the properties of cementite at the nanoscale is essential in the study and design of new steels. Atomistic simulation methods, such as molecular dynamics (MD) or Monte Carlo simulations, offer an efficient and reliable route to investigate nanoscale mechanics pertaining to cementite in steel alloys. Each of these methods requires accurate interatomic potentials to find the energy of the system under investigation. However, first-principles calculations – albeit rigorous and accurate – are incapable of simulating the large number of atoms required for realistic calculations due to unreasonable memory and processing time requirements. Given this limitation the best solution is to use a higher length scale simulation such as classical MD simulations via interatomic potential models.

Among the spectrum of semiempirical formulations, the modified embedded atom method (MEAM) originally proposed by Baskes (1992) has been shown to accurately predict the properties of most crystal structures, such as bcc, fcc, hcp, and even diatomic gases, in good agreement with experiments or first-principles calculations. MEAM was extended from the embedded atom method (EAM) (Daw and Baskes, 1984) to include the directionality of bonds. In the original MEAM formalism, only the first-nearest neighbor (1NN) interactions were considered (Baskes, 1992). Lee and Baskes later extended the original formalism to include the screened second-nearest neighbor (2NN) interactions (Lee *et al.*, 2001). Further details of the MEAM formalism can be found in Baskes (1992) and Lee *et al.* (2001).

One of the commonly used 2NN MEAM potentials for the Fe–C system developed by Lee (2006) was designed to predict the interactions of interstitial C atoms with defects, such as vacancies. According to Fang *et al.* (2012), Lee's potential predicts that cementite is stable only up to a temperature of 750 K (Fang *et al.*, 2012). Experimentally, however, cementite is metastable with a positive heat of formation (Meschel and Kleppa, 1997) and only decomposes between 1100 and 1200 K (Callister and Rethwisch, 2007; Henriksson and Nordlund, 2009). Among recent interatomic potentials (Becquart *et al.*, 2007; Lau *et al.*, 2007; Hepburn and Ackland, 2008; Ruda *et al.*, 2009; Henriksson and Nordlund, 2009) for the Fe–C system, EAM potentials by Lau *et al.* (2007) and Ruda *et al.* (2009) and the short-ranged Tersoff–Brenner type analytical bond order potential (ABOP) by Henriksson and Nordlund (2009) all promise to predict the properties of cementite reasonably well. In the potentials by Lau *et al.* (2007) and Ruda *et al.* (2009), however, the single-element potential for C does not predict the properties of both graphite and diamond well. This is due to the limited ability of EAM to describe the bare C–C interaction correctly (Duff and Sluiter, 2010). We note that a successful interatomic potential for an alloy system should not only predict the properties of the alloy correctly, but it should also predict the properties of the individual alloying elements in their natural crystal structures accurately. The ABOP by Henriksson and Nordlund (2009) accurately predicts the properties of cementite as well as Fe and C; however, ABOPs are not applicable to simulations involving interfaces and surfaces (Erhart *et al.*, 2006). Furthermore, ABOPs are restricted to 1NN interactions only (Erhart *et al.*, 2006; Albe *et al.*, 2002).

In this chapter, we develop a 2NN MEAM potential model for the Fe–C alloy system by optimizing the MEAM parameters to reproduce the structural and elastic properties of cementite as predicted by density functional theory (DFT), which is a method to calculate the electronic structures and their attributes. Our Fe–C alloy potential is based on previously developed 2NN MEAM potentials for Fe (Lee *et al.*, 2012) and C (Uddin *et al.*, 2010) in their pure forms. The MEAM potential for C predicts both diamond and graphite

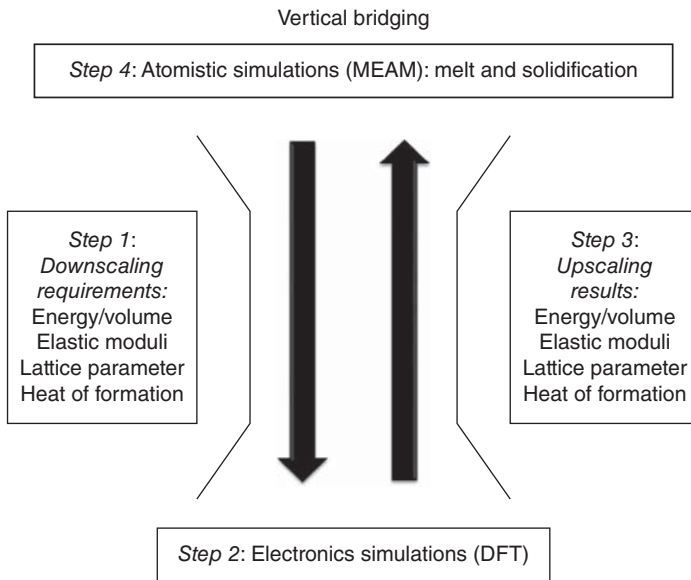


Figure 2.1 Schematic showing the sequence of steps in vertical bridging between the smallest length scale (electrons) and the next higher length scale (atoms) for examining the formation of cementite.

as stable structures with nearly degenerate energies. Using the Fe and C single-element potentials, we obtained the most optimal parameterization of the alloy potential of Fe–C for the purposes specified by the objective function that takes into account various properties of Fe–C alloys. We validate the final MEAM parameterization for cementite by predicting its melting temperature through MD simulations within a few Kelvin of the experimental value. Downscaling requires that the MEAM potential receive the following information for calibration from the DFT results as shown in Figure 2.1: elastic moduli, energy per unit volume, and the lattice parameter. See Horstemeyer *et al.* (2015) for the formal procedure. Once these are calibrated, then one can validate and optimize the parameters with other characteristics of importance, that is, heat of formation, generalized stacking faulty energy curves, and so on.

2.2 Methods

In order to perform a MD simulation involving thousands to millions of atoms, the interactions between atoms have to be described by an interatomic potential model. In our case, that model is MEAM. In the MEAM formalism,

the total energy of the system is given by

$$E = \sum_i F^i \left(\sum_{i \neq j} \rho^i [r^{ij}] \right) + \frac{1}{2} \sum_{ij} \varphi^{ij} [r^{ij}] \quad (2.1)$$

where atom i has j neighboring atoms with r^{ij} separation and the pair potential between atom i and atom j is φ^{ij} (Baskes, 1992). The functional form of MEAM uses experimental or first-principles data such as cohesive energy and equilibrium neighbor distance, as well as parameters that are determined through fitting to the properties such as elastic constants and defect energies obtained from experiments or first-principles calculations. Therefore, the downscaling requirements from the atomic level are the material properties needed to parameterize MEAM. The focus of the current study is cementite, which is a metastable phase in the Fe–C phase diagram. In order to capture cementite’s transition temperatures and structures, it is essential that the MEAM potential can predict a few more phases other than cementite. Therefore, we start out with Fe and C MEAM potentials that correctly predict their phase stabilities (see Section 2.3). Then, we use a novel optimization method (described in Section 2.4) to optimize the Fe–C alloy MEAM parameterization to reproduce properties of cementite and other Fe–C structures, summarized in Table 2.4. The properties are prioritized in the order they appear in Table 2.4. The first receives the highest and the last receives the lowest priority in the form of weighting factor.

2.2.1 MEAM Calculations

For all atomic-scale simulations described in this chapter, we use MEAM as implemented in LAMMPS, the classical MD simulation code developed at Sandia National Laboratories (Plimpton, 1995; Plimpton *et al.*, 2011). Furthermore, we compare the results of our current potential with published potentials of Ruda *et al.* (2009), Lee (2006), and Henriksson and Nordlund (2009).

2.2.2 DFT Calculations

Reference material properties needed in the fitting of the MEAM Fe–C potential such as of single-crystal cementite, hypothetical structures (Fe–C in B_1 , L_{12}), and C interstitials (octahedral and tetrahedral) in bcc Fe were calculated using the first-principles method DFT as implemented in the Vienna Ab initio Software Package (VASP) (Kresse and Hafner, 1993; Kresse and Furthmüller, 1996). DFT is a first-principles method that is derived from the quantum mechanical description of materials, which requires no parameterization or fitting. It is one of the most rigorous first-principles methods used to calculate material properties. The interaction between valence electrons and positive

ions shielded by core electrons are represented by Projector Augmented Wave (PAW) pseudopotentials (Kresse and Joubert, 1999). Electron exchange and correlation in DFT were treated within the generalized gradient approximation (Perdew *et al.*, 1996). Brillouin zone sampling was performed using the Monkhorst–Pack scheme (1976) with a Fermi-level smearing of 0.2 eV applied using the Methfessel–Paxton method (1989). Geometric optimizations were carried out using the conjugate gradient minimization method (Kresse and Hafner, 1993).

2.3 Single-Element Potentials

The single-element MEAM potential parameters used in this work are presented in Table 2.1. The parameters for Fe are from the MEAM potential developed by Lee *et al.* (2012) and the parameters for C are from Uddin *et al.* (2010). The single-element MEAM calibration methodology is given in Horstemeyer *et al.* (2015) and tutorials are given at <http://icme.hpc.msstate.edu> under nanoscale.

2.3.1 Energy versus Volume Curves

Energy variation with respect to volume or nearest neighbor distance is considered an important test of validity for interatomic potentials. Here, we present the energy versus volume curves generated by the single-element potential for Fe and energy versus nearest neighbor distance curves generated by the single-element potential for C. Figure 2.2 shows the energy versus volume curve for bcc Fe in comparison with curves generated by DFT calculations as well as by using experimental data. It is well known that DFT overestimates the cohesive energy (Philipsen and Baerends, 1996). Therefore, the DFT curve is shifted vertically by a constant amount to the experimental cohesive energy at the equilibrium volume to aid the comparison of the curves. Due to overbinding, the DFT's prediction for the equilibrium volume is underestimated (Devey and de Leeuw, 2010). Therefore, the DFT curve sits to the left of the experimental curve. The experimental curve was generated through Rose's equation of state (Rose *et al.*, 1984) (Eq. (2.1)) using the experimental bulk modulus, cohesive energy, and atomic volume at equilibrium listed in Table 2.2. We also tested the stability of Fe in several different crystal structures including body-centered cubic (bcc), face-centered cubic (fcc), and hexagonal closed packed (hcp) structures as shown in Figure 2.2. The Fe MEAM potential correctly predicts that bcc is the most stable structure, as observed in experiment and by the first-principles methods. MEAM predicts that fcc and hcp Fe are much closer in energy and have a larger volume than that calculated from DFT.

Table 2.1 Set of the MEAM potential parameters for pure Fe (by Lee *et al.* (2012)) and C (by Uddin *et al.* (2010)).

Element	E_c	r_e	r_{cut}	A	α	a_3	ρ_0	$\beta^{(0)}$	$\beta^{(1)}$	$\beta^{(2)}$	$\beta^{(3)}$	$t^{(0)}$	$t^{(1)}$	$t^{(2)}$	$t^{(3)}$	C_{min}	C_{max}
Fe	4.28	2.469	4.5	0.585	5.027	0.3	1.0	3.8	2.0	0.9	0.0	1.0	-0.8	12.3	2.0	0.68	1.9
C	7.37	1.545	4.5	1.49	4.38	0.0	1.0	4.26	5.0	3.2	3.98	1.0	7.5	1.04	1.01	2.0	2.8

The bcc and diamond lattices are chosen as the reference structures for Fe and C, respectively. See Ref. Baskes (1992); Lee *et al.* (2001) for the meaning of each parameter.

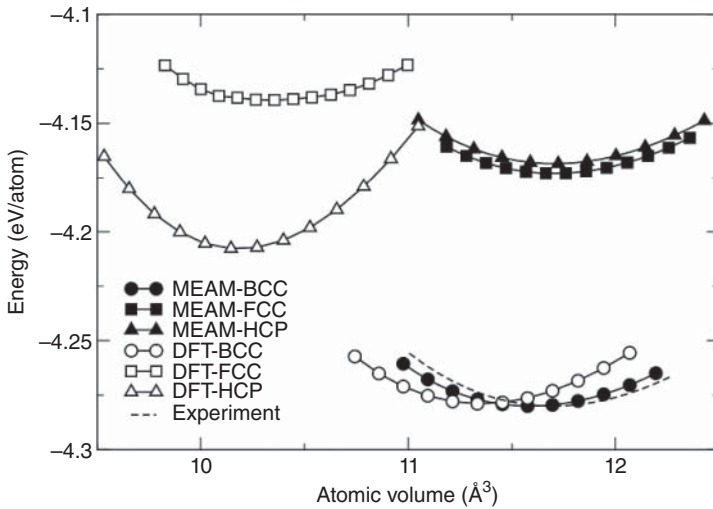


Figure 2.2 Energy versus volume curves for Fe in bcc, fcc, and hcp crystal structures. The solid curve is constructed from experimental values in Table 2.2. For ease of comparison, the DFT curves are shifted vertically by a constant amount equal to the difference between experimental and DFT cohesive energies of Fe in bcc at equilibrium volumes.

The single-element MEAM potential for C predicts both diamond and graphite to be stable structures. The energy versus nearest neighbor distance curves for diamond and graphite are shown in Figure 2.3.

The experimental curves were constructed from Rose's equation of state (Rose *et al.*, 1984) (Eq. (2.1)) using the experimental bulk modulus, cohesive energy, and nearest neighbor distance at equilibrium, as listed in Table 2.2. MEAM predictions for diamond are in good agreement with the experimental results. MEAM predicts almost degenerate cohesive energies for graphite and diamond, while DFT predicts graphite to be ~ 0.1 eV more stable than diamond. For graphite, DFT predicts a 1NN distance in good agreement with experiment, while MEAM predicts a 1NN distance $\sim 3\%$ greater than the experimental value. The experimental ratio between lattice parameters c and a in graphite (hereafter referred to as c/a ratio) is 2.725 (Yin and Cohen, 1984). MEAM optimized the c/a ratio of the graphite structure to 3.35. The disagreement between experimental and MEAM values for c/a ratio is due to the incorrect prediction of interlayer interaction of graphite, which is dominated by van der Waals forces that are not described by the MEAM potential. However, the dependence of cohesive energy on the c/a ratio is small. Figure 2.4 shows the change in energy as c is varied while keeping a at the MEAM optimized value. According to Figure 2.3, the difference in cohesive energy of graphite between the experimental and MEAM c/a ratio is ~ 4 meV/atom. In constructing the energy versus nearest neighbor

Table 2.2 Material properties predicted by the single-element MEAM potentials.

Property	bcc Fe	Diamond	Graphite
E_c	-4.28(-4.28) ^{a)}	-7.37(-7.37) ^{c)}	-7.369(-7.374) ^{d)}
B	175(166–173) ^{b)}	443(443) ^{c)}	176(286) ^{d)}
a	2.86(2.86) ^{b)}	3.567(3.567) ^{c)}	2.53(2.461) ^{d)}
c	—	—	2.476(6.709) ^{d)}
Ω_0	11.64(11.70)	5.67(5.67)	11.75(2.80)

E_c is the cohesive energy (eV/atom); a and c are the equilibrium lattice constants (Å); B is the bulk modulus (GPa); and Ω_0 is the equilibrium atomic volume (Å³/atom). Experimental data are given in parentheses. Experimental values for equilibrium atomic volume were calculated from the experimental lattice parameter(s).

a) Kittel (1986) as reported by Lee *et al.* (2012).

b) As reported by Lee *et al.* (2012).

c) Donohue (1982); McSkimin *et al.* (1972) as reported by Fahy and Louie (1987).

d) Murnaghan (1944) as reported by Yin and Cohen (1984).

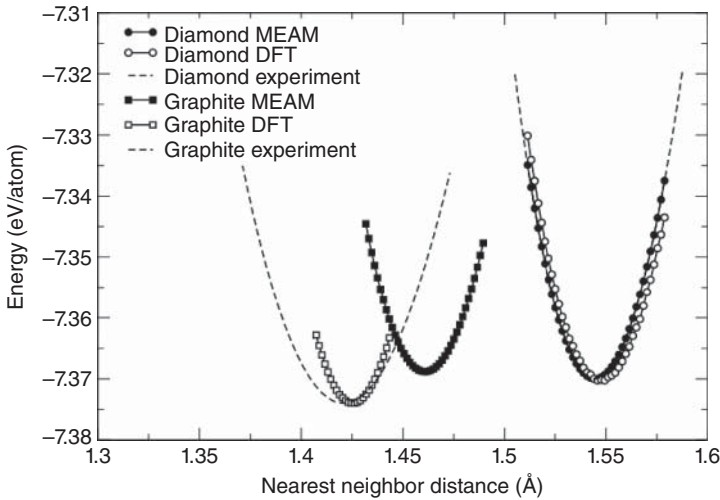


Figure 2.3 Energy versus nearest neighbor distance curves for C in diamond and graphite. The solid curve is constructed from experimental values in Table 2.2. For comparison, the DFT curve is shifted vertically to the experimental cohesive energy at the equilibrium nearest neighbor distance.

distance curves for graphite, the interplanar distance was scaled with the lattice constant. The experimental ratio was used in the generation of the DFT curve, while the MEAM curve was constructed with the predicted c/a ratio.

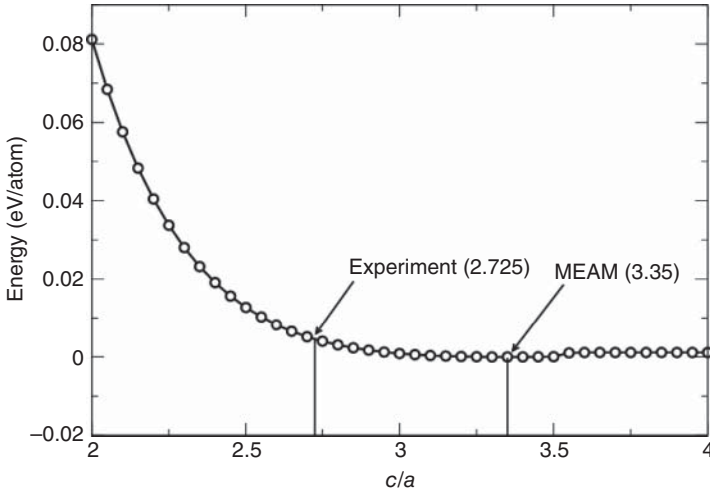


Figure 2.4 Cohesive energy of graphite as a function of the c/a ratio. Energy at zero is set to the minimum energy predicted by the MEAM potential.

2.3.1.1 Single-Element Material Properties

The cohesive energy, equilibrium lattice constants, and bulk moduli for bcc Fe, graphite, and diamond were determined by fitting Rose's equation of state (Rose *et al.*, 1984) to the energy versus nearest neighbor distance/volume curves generated by MEAM.

$$E_i^u = -E_i^0 \left(1 + a^* + a_3 \frac{a^{*3}}{R/R_i^0} \right) e^{-a^*} \quad (2.2)$$

$$a^* = \alpha_i \left(\frac{R}{R_i^0} - 1 \right) \quad (2.3)$$

$$\alpha_i^2 = 9B_i\Omega_i/E_i^0 \quad (2.4)$$

R_i^0 is the equilibrium nearest neighbor distance, E_i^0 is the cohesive energy, B_i is the bulk modulus, Ω_i is the equilibrium atomic volume, and a_3 is the coefficient of the cubic term. a_3 is set to zero when fitting to energy versus nearest neighbor distance/volume curves generated by MEAM. The single-element material properties compared to experimental values are given in Table 2.2.

2.4 Construction of Fe-C Alloy Potential

Table 2.3 lists the parameters in the 2NN MEAM potential for Fe-C alloy system optimized by following the general framework developed by

Table 2.3 The optimized parameters in the 2NN MEAM potential for Fe–C alloy system.

Parameters	Values
Δ	0.002
r_e	1.92
R_{cut}	4.5
α	4.75
a_3	0.125
ρ_0 (Fe)	1.0
ρ_0 (C)	5.49
C_{max} (Fe,Fe,C)	2.8
C_{max} (Fe,C,C)	2.8
C_{max} (Fe,C,Fe)	2.8
C_{max} (C,C,Fe)	2.8
C_{min} (Fe,Fe,C)	0.06
C_{min} (Fe,C,C)	2.0
C_{min} (Fe,C,Fe)	2.0
C_{min} (C,C,Fe)	0.5

The triplet (A,B,C) represents the configuration with C atom in between A and B atoms. The B_1 lattice is chosen as the reference structure.

Tschopp *et al.* (2012). The framework consists of two stages. The first stage, called the global approach (GA), is a coarse refinement of the parameter space of the MEAM potential, which initializes the MEAM potential parameters and performs a sensitivity analysis for the parameters. The second stage, called the local approach (LA), evaluates the sensitive parameters sampling the parameter space with a stratified sampling method and generates analytical models for design optimization of the potential.

In the GA stage, a coarse refinement of the parameter space is performed using a partial set of the properties in the objective function including the heats of formation of cementite, Fe_3C in L_{12} structure and FeC in B_1 structure, and the interstitial energies of C in the bcc Fe lattice at octahedral and tetrahedral positions. The potential parameters were initialized as specified by the MEAM formulation (Baskes, 1992; Lee *et al.*, 2001). α defined by Eq. (2.3) and r_e (equilibrium nearest neighbor distance) are determined by the reference structure properties. For the present case, FeC in the B_1 structure is used as

the reference structure, and the values predicted by DFT are used to set α and r_e since experimental values are not available for this hypothetical structure. Parameters α and r_e remain unchanged throughout the optimization process, since they are defined by the MEAM formulation. Next, a sensitivity analysis was performed to evaluate the influence of each parameter on the properties. This step helps identify parameters with the most significant effect on the selected target properties of the Fe–C system. By identifying the parameters that have the most influence on the properties of the Fe–C system, we are able to reduce the number of parameters to be included in the later stages. For this case, the GA stage identified five parameters – Δ , a_3 , $\rho_0(\text{C})$, $C_{\min}(\text{Fe}, \text{Fe}, \text{C})$, and $C_{\min}(\text{C}, \text{C}, \text{Fe})$ – to be sufficiently sensitive to be further explored in the LA stage of the optimization. Parameters that are deemed insensitive are fixed at the default values recommended in the MEAM formulation. In addition to identifying the sensitive parameters, the range of sensitivity of these parameters was determined. The variation of the sensitive parameters in their most sensitive range can be observed in Figure 2.5. From these plots, additional information can be extracted. For instance, only the Δ parameter has an effect on the heat of formation of Fe–C in B_1 , whereas the heat of formation of Fe–C in L_{12} is not as sensitive to $C_{\min}(\text{C–C–Fe})$ as it is sensitive to other parameters. The results of the sensitivity analysis suggest the existence

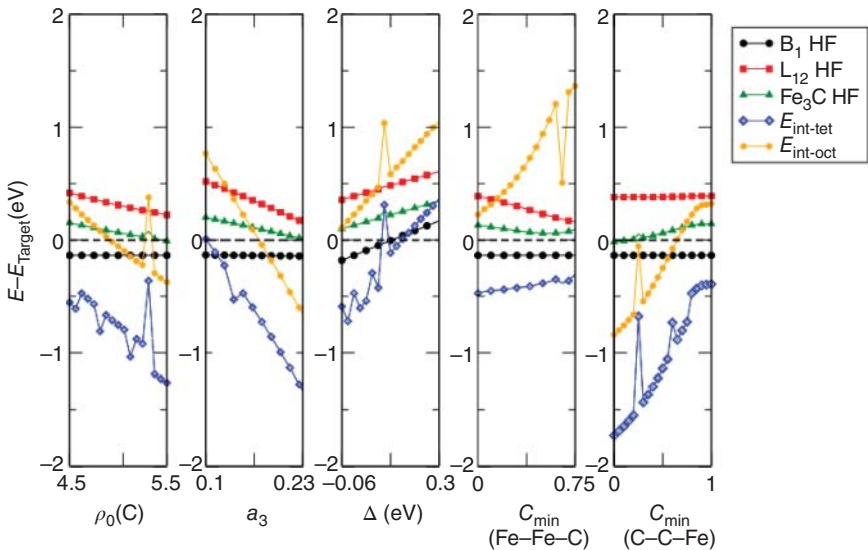


Figure 2.5 Sensitivity (change in target versus range of sensitivity) of selected properties of the Fe–C system: Heat of formation (HF) of Fe–C in the B_1 (B_1 HF) and L_{12} structure (L_{12} HF), HF of cementite (Fe_3C HF), interstitial energies of C in bcc Fe in tetrahedral ($E_{\text{int-tet}}$) and octahedral positions ($E_{\text{int-oct}}$).

of nonlinear correlations between potential parameters that are critical in interatomic potential construction.

The LA stage of the potential optimization procedure involves sampling the bounded potential parameter space, generating analytical models that represent the nonlinear correlations between the potential parameters, and using an objective function to converge on the required parameterization of the potential.

A stratified random sampling method known as Latin Hypercube Sampling (LHS) (McKay *et al.*, 2000) was used to sample the potential parameter space with 4000 different potential parameter combinations. The set of properties chosen for the Fe–C system are calculated for each parameter combination. This is the most computationally intensive step of the potential fitting process. Figure 2.6 elaborates the relationship between the sensitive potential parameters and the target energies by illustrating the evolution of heat of formation of cementite as a function of the sensitive potential parameters. Multiple data points are generated for a single value of a specific potential parameter. This

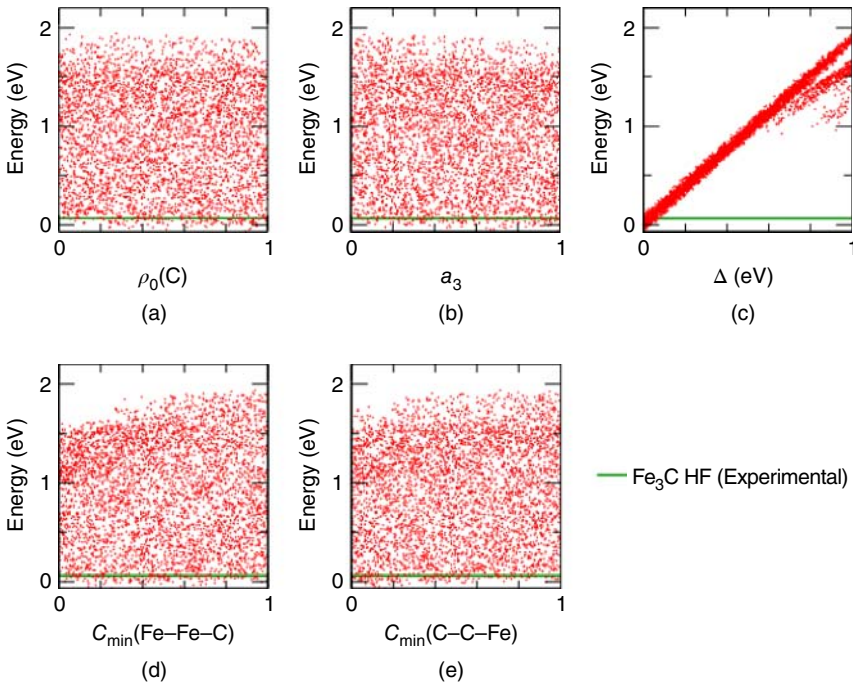


Figure 2.6 Heat of formation of cementite as a function of (a) density scaling factor ρ_0 , (b) additional cubic term in the universal energy equation a_3 , (c) heat of formation of the reference structure Δ (eV), and angular screening parameters, (d) $C_{\min}(\text{Fe-Fe-C})$ and (e) $C_{\min}(\text{C-C-Fe})$.

is due to LHS changing the other four parameters for a single value of the parameter in consideration. According to Figure 2.6(c), the Δ parameter has a much larger effect on the heat of formation of cementite compared to the other four parameters. This is true for the other target energies as well. Since Δ is the heat of formation of the alloy potential reference structure, its effect on energies is much larger.

Using the data from the parameter space sampling step, analytical models representing the relationship between potential parameters and the selected target properties are generated. This is done by fitting higher-order polynomial regression models to the sampled data. The analytical models represent a response surface for the sensitive potential parameters. At this stage of the optimization, an objective function representing all of the relevant properties of the Fe–C system is introduced. The objective function is constructed by combining the weighted differences between the MEAM predicted values and the target values of the chosen properties. Target values are set to experimental values when available or DFT values otherwise. Then, a constrained nonlinear optimization procedure is used to evaluate the analytical models by minimizing the objective function.

The properties included in the objective function are the properties of cementite (equilibrium lattice parameters and volume, heat of formation, elastic constants, and surface formation energies); properties of Fe_3C in L_{12} structure (heat of formation and equilibrium volume); properties of FeC in B_1 structure (heat of formation, equilibrium volume and elastic constants), and interstitial defect energies of C in the bcc Fe lattice at octahedral and tetrahedral positions. The weighting factors of the objective function balance the trade-offs in potential optimization. The purpose of this work is to model the properties of cementite while reproducing the Fe–C alloy system properties to an acceptable accuracy. This is realized by choosing weighting factors in a way that cementite properties were prioritized first, then the interstitial defect energies, and then the properties of hypothetical structures B_1 and L_{12} . By varying the weighting factors, the objective function is changed and the constrained nonlinear optimization procedure can traverse the response surface represented by the analytical models to obtain a final set of potential parameters. For each set of weighting factors, a potential is generated. By using a matrix of weighting factors with the required prioritization of the target properties, we were able to minimize the objective function and arrive at the set of optimal potential parameters in Table 2.3. The optimized potential is then validated by predicting material properties that were not used in the optimization procedure. We used the melting temperature of cementite to validate the potential and its prediction is described in Section 2.2. Table 2.4 shows the material properties predicted by the present MEAM potential compared with DFT/experimental data and the values from other existing potentials.

Table 2.4 Comparison of the present MEAM potential with DFT/experimental data and potentials by Lee (2006), Ruda *et al.* (2009) and Henriksson and Nordlund (2009).

Properties	DFT/Expt	MEAM	Lee ^{a)}	Ruda ^{b)}	Henriksson ^{c)}
<i>Cementite</i>					
ΔH_f (eV/atom)	0.01(0.05 ^{d)})	0.06	0.02 ^{e)} , -0.015 ^{f)}	0.18	0.03
Ω_0 (\AA^3 /atom)	9.56 ^{g)} (9.67 ^{e)})	9.49	9.5	9.11	9.33
<i>Lattice parameters</i> (\AA)					
A	5.06 ^{g)} (5.08 ^{h)})	5.05	5.16	5.14	5.09
B	6.70 ^{g)} (6.73 ^{h)})	6.69	6.32	6.52	6.52
C	4.51 ^{g)} (4.52 ^{h)})	4.49	4.66	4.35	4.5
<i>Elastic constants</i> (GPa)					
C_{11}	388 ⁱ⁾	322		263	363
C_{22}	345 ⁱ⁾	232		219	406
C_{33}	322 ⁱ⁾	326		247	388
C_{12}	156 ⁱ⁾	137		176	181
C_{23}	162 ⁱ⁾	118		143	130
C_{13}	164 ⁱ⁾	170		146	166
C_{44}	15 ⁱ⁾	17		77	91
C_{55}	134 ⁱ⁾	103		95	125
C_{66}	134 ⁱ⁾	64		123	134
<i>Polycrystalline moduli</i>					
B (GPa)	224(174 \pm 6 ^{j)})	188		183	234
G (GPa)	72(74 ^{k)})	56		69	114
Y (GPa)	194(177 ^{l)} , 196 ^{m)} , 200 ^{k)})	153		184	293
ν	0.36(0.36 ^{k)})	0.36		0.33	0.29
<i>Surface energies</i> (J/m ²)					
$E_{[001]}$	2.05 ⁿ⁾	2.05		1.96	
$E_{[010]}$	2.26 ⁿ⁾	1.8		2	
$E_{[100]}$	2.47 ⁿ⁾	2.01		2.34	
<i>Interstitial energies</i> (eV) (C in bcc Fe)					
$E_{\text{Tetrahedral}}$	2.14	1.76		2.08	1.5
$E_{\text{octahedral}}$	1.25	1.55		1.81	1.18
<i>Hypothetical structures</i>					
$\Delta H_f B_1$ (eV/atom)	0.53	0.002			
$\Omega_0 B_1$ (\AA^3 /atom)	7.97	7.08	2.49		
$\Delta H_f L_{12}$ (eV/atom)	0.72	0.66			
$\Omega_0 L_{12}$ (\AA^3 /atom)	10.27	10.05			

Table 2.4 (Continued)

Properties	DFT/Expt	MEAM	Lee ^{a)}	Ruda ^{b)}	Henriksson ^{c)}
B ₁ elastic constants (GPa)					
C ₁₁	601	566	550 ^{o)}		
C ₁₂	589	213	228 ^{o)}		
C ₄₄	83	145	33 ^{o)}		

ΔH_f is the heat of formation, Ω_0 is the equilibrium volume, B is polycrystalline bulk modulus, G is polycrystalline shear modulus, Y is polycrystalline Young's modulus, and ν is polycrystalline Poisson's ratio.

- a) Lee (2006).
- b) Ruda *et al.* (2009).
- c) Henriksson and Nordlund (2009).
- d) Meschel and Kleppa (1997).
- e) Lee (2006).
- f) Fang *et al.* (2012).
- g) Shein *et al.* (2006).
- h) Wood *et al.* (2004) as cited by Shein *et al.* (2006).
- i) Data of relaxed calculations Jiang *et al.* (2008).
- j) Li *et al.* (2002).
- k) Laszlo and Nolle (1959).
- l) Mizubayashi *et al.* (1999).
- m) Umemoto *et al.* (2001).
- n) Chiou (2003).
- o) Private communication with B.-J. Lee.

2.5 Structural and Elastic Properties of Cementite

Structural properties of cementite including the equilibrium lattice parameters, the equilibrium volume per atom, and the heat of formation are presented in Table 2.4 with comparison to DFT/experiment and other interatomic potentials. Our prediction of the heat of formation of cementite is in good agreement with DFT and experimental data. Lee's and Henriksson's potentials also predict values in good agreement with DFT and experiment, while Ruda's potential predicts a much larger value. Lattice constants of the present MEAM and literature potentials (Lee, 2006; Ruda *et al.*, 2009; Henriksson and Nordlund, 2009) agree well with experiment, while DFT predicts lower values.

To verify the results, the variation of cohesive energy with volume was calculated. Figure 2.7 compares the energy versus volume curves for cementite generated by the present MEAM potential with DFT and experimental curves. During volume variation of cementite, the ratios among a , b , and c lattice parameters were held constant. As noted before, DFT overestimates the cohesive energy and underestimates the equilibrium volume. Therefore,

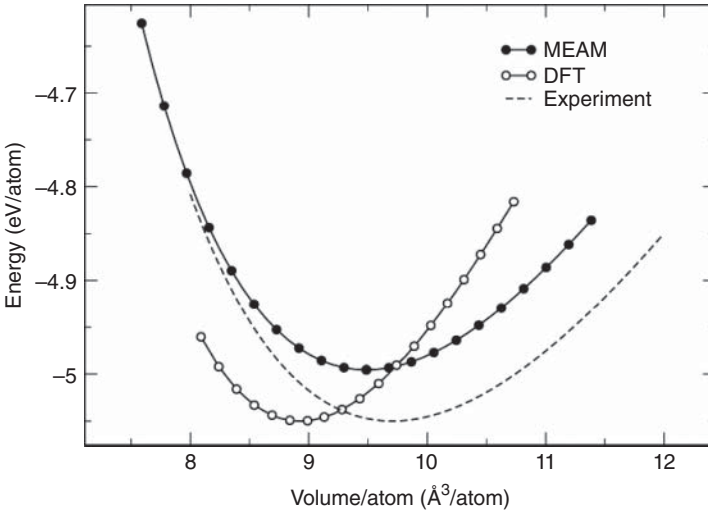


Figure 2.7 Comparison of energy versus volume curves for cementite. The dashed-line curve is constructed from experimental values of the cohesive energy, equilibrium volume and polycrystalline bulk modulus, of cementite. For comparison, the DFT curve is shifted vertically to the experimental cohesive energy at the equilibrium volume.

the DFT curve sits to the left of the experimental curve, and it is shifted vertically to the experimental cohesive energy at the equilibrium volume to aid the comparison. The experimental curve was generated by Murnaghan's equation of state (Murnaghan, 1944, 1967)

$$E(V) = E(V_0) + \frac{B_0 V}{B'_0(B'_0 - 1)} \times \left[B'_0 \left(1 - \frac{V_0}{V} \right) + \left(\frac{V_0}{B'_0} \right)^{B'_0} - 1 \right] \quad (2.5)$$

with the experimental bulk modulus B_0 (Li *et al.*, 2002), its derivative B'_0 (Li *et al.*, 2002), volume V_0 (Umemoto *et al.*, 2001), and cohesive energy $E(V_0)$ (Meschel and Kleppa, 1997). The experimental single-crystal bulk modulus of cementite has not yet been determined; therefore, the polycrystalline bulk modulus of cementite was used to generate the experimental curve.

2.5.1 Single-Crystal Elastic Properties

The elastic moduli of cementite were calculated and compared to DFT and the interatomic potentials by Ruda *et al.* (2009), and Henriksson and Nordlund (2009) as presented in Table 2.4. They were calculated using the deformation matrix presented in Jiang *et al.* (2008). In linear elastic theory, deformation energy is a function of strain. Distortion energies (ΔE) calculated for strains (δ) equal to $\pm 0.5\%$ were fitted to $\Delta E = k_2 \delta^2 + k_3 \delta^3$. DFT calculations

were performed for $\delta = \pm 2\%$ (Jiang *et al.*, 2008). The single-crystal elastic constants were obtained using the relationships for the quadratic coefficient k_2 listed in Jiang *et al.* (2008). These results show that the present MEAM potential for Fe–C alloy predicts cementite to be stable (positive elastic constants) and their values are reasonably close to those predicted by DFT. Specifically, the present MEAM potential reproduces the low value of C_{44} reported by DFT, which none of the other interatomic potentials were able to do (MEAM C_{44} of 17 GPa versus DFT C_{44} 15 GPa).

2.5.2 Polycrystalline Elastic Properties

The theoretical upper and lower bounds for the polycrystalline bulk modulus (B) and shear modulus (G) were calculated using the single-crystal elastic constants according to methods by Reuss and Voigt (Panda and Chandran, 2006; Jiang *et al.*, 2008). The polycrystalline B and G were then estimated using Hill's average (Hill, 1952; Jiang *et al.*, 2008). Young's modulus (Y) and Poisson's ratio (ν) were calculated by using (Jiang *et al.*, 2008).

$$Y = 9BG/[3B + G] \quad (2.6)$$

$$\nu = [3B/2 - G]/[3B + G] \quad (2.7)$$

Polycrystalline elastic moduli predicted by the present MEAM potential are presented in Table 2.4, in comparison with DFT, experiment, and interatomic potentials by Ruda *et al.* (2009) and Henriksson and Nordlund (2009). The elastic constants predicted by DFT are in good agreement with experiment. The present MEAM potential gives the best agreement with experiment among the three interatomic potentials for B and ν ; the present MEAM predicts the ν value equal to the experimental value. Ruda's potential predicts the best agreement with experiment for G and Y .

2.5.3 Surface Energies

Calculations were performed on [001], [010], and [100] surfaces to determine the surface formation energy. Table 2.4 compares the surface formation energies of the present MEAM to DFT (Chiou, 2003) and the interatomic potential by Ruda *et al.* (2009). The atoms near the surfaces are fully relaxed to allow reconstruction if necessary. The predicted surface energies have the same order of magnitude as DFT results. However, the present MEAM results give a wrong order of stability among the three surfaces. Although this minor shortcoming could cause the present MEAM potential to predict incorrect distributions of surface orientations for cementite clusters, it would not affect the efficacy of the present MEAM potential as its main purpose is to predict the correct bulk properties of Fe–C alloys.

2.5.4 Interstitial Energies

The interstitial point defect formation energy E_{int} is given by

$$E_f^{\text{int}} = E_{\text{tot}}[\text{N} + \text{A}] - E_{\text{tot}}[\text{N}] - \epsilon_{\text{A}} \quad (2.8)$$

where the total energy of a system with N (Fe or C) atoms is $E_{\text{tot}}[\text{N}]$ and $E_{\text{tot}}[\text{N} + \text{A}]$ is the total energy of a system with N atoms plus the inserted atom A (Fe or C), and ϵ_{A} is the total energy per atom of type A in its most stable bulk structure. In this case, we considered interstitial defects of C atoms in a Fe bcc lattice. Interstitial defect formation energies of C at the octahedral and tetrahedral positions of the Fe bcc lattice were calculated. The results are presented in Table 2.4 with comparison to DFT results, and to other interatomic potentials. The present MEAM potential predicts the octahedral defect to be the most stable in agreement with DFT results. However, the difference between two defect energies is smaller compared to that of DFT.

2.6 Properties of Hypothetical Crystal Structures

The heat of formation of Fe–C in B_1 crystal structure and L_{12} crystal structure as well as their equilibrium volumes are also presented in Table 2.4. The heat of formation of B_1 is unusually low compared to DFT results. B_1 is the reference structure of the Fe–C alloy potential and its heat of formation is defined by the Δ parameter of the potential. The Δ parameter also has a large effect on the heat of formation of cementite and thereby to its structural and elastic properties. Heats of formation of B_1 and L_{12} are used as target properties in the GA stage of the potential construction process. However the heats of formation of these two structures are weighted far less in the construction of the objective function for obtaining the final potential parameters as compared to properties of cementite. This caused the Δ parameter to have a low value to reproduce overall cementite properties with greater accuracy. This should not pose a serious problem since B_1 is a hypothetical structure for Fe–C and does not naturally occur.

2.6.1 Energy versus Volume Curves for B_1 and L_{12} Structures

The cohesive energy of Fe–C in the B_1 and L_{12} crystal structures as a function of the atomic volume is shown in Figures 2.8 and 2.9, respectively. For the B_1 structure, the present MEAM potential predicts an atomic volume $\sim 11\%$ less and a bulk modulus $\sim 0.3\%$ less than DFT. The MEAM prediction for the L_{12} structure gives an atomic volume $\sim 11\%$ greater, and a bulk modulus 35% less than DFT. As mentioned earlier, DFT overestimates the cohesive energy. Therefore, to aid the comparison in these figures, the DFT curves are shifted